

A COMPOSITE WING DESIGN APPROACH FOR
GUST ENERGY HARVESTING THROUGH
AEROELASTIC TAILORING

by

Korbin C. Mallette

Bachelor of Engineering, Toronto Metropolitan University (2022)

A thesis

presented to Toronto Metropolitan University

in partial fulfillment of the

requirements for the degree of

Master of Applied Science

in the program of

Aerospace Engineering

Toronto, Ontario, Canada, 2025

© Korbin C. Mallette 2025

AUTHOR'S DECLARATION FOR ELECTRONIC SUBMISSION OF A THESIS

I hereby declare that I am the sole author of this thesis. This is a true copy of the thesis, including any required final revisions, as accepted by my examiners.

I authorize Toronto Metropolitan University to lend this thesis to other institutions or individuals for the purpose of scholarly research.

I further authorize Toronto Metropolitan University to reproduce this thesis by photocopying or by other means, in total or in part, at the request of other institutions or individuals for the purpose of scholarly research.

I understand that my thesis may be made electronically available to the public.

A Composite Wing Design Approach for Gust Energy Harvesting through Aeroelastic Tailoring

Korbin C. Mallette

Master of Applied Science, Aerospace Engineering, Toronto Metropolitan University,
Toronto (2025)

Abstract

This thesis proposes a structural design approach to implement gust energy harvesting through aeroelastic tailoring into the design of an aircraft. Gust energy harvesting through aeroelastic tailoring allows for the energy extracted from a turbulent atmosphere while traversing a gusty environment to be increased, resulting in a net drag reduction while within upward and downward gusts. An increase in energy altitude gains of 6.1% was shown to be achievable purely through structural design for an aircraft traversing a gust with net-zero effect on the airmass. It was shown that by applying the proposed design method an aeroelastically tailored composite structure can be selected that has increased energy altitude gains through a gust with minimal weight penalties.

Acknowledgments

The research presented in the following thesis was made possible through the support of Superwake LTD with special thanks to Micheal and Devin. You both supported me through the sharing of your knowledge, insight, and skills and I am forever thankful for the opportunity you have given me to develop this research and my personal skills. I would like to thank the rest of the Superwake crew for supporting me through this journey, and for Eric keeping me sane.

I would like to thank Dr. Goetz Bramesfeld and Dr. Kazem Fayazbakhsh for their support and immensely helpful guidance and insight through this work. I was insanely lucky to have been taken into your lab, Dr.Bramesfeld, in my second year and I am glad that it has lead to this research. Thank you for your help and the confidence put in me to help me develop my skills as a researcher, academic, and my ability to apply these skills to a variety of applications through CREATeV and Superwake. Dr.Fayazbakhsh, I cannot thank you enough for your help throughout my work here and the guidance you have provided me with regards to structures and composites. Thank you for your time and your invaluable knowledge.

Dr. Julia Cole, you have been a wonder in the later parts of this research, and I cannot begin to thank you for the writing, academic direction, and personal advice you have provided me. If it were not for your insight I am convinced I would not be reaching this point. I am insanely lucky to have met you and you are a credit to the concept of kindness.

Apart from the aid provided to me through other academics I of course would not have made it here without the support of my family. My parents have listened to my overly-dramatic woes throughout my time here and I will forever be grateful. And of course Lucas, my brother, has provided welcome and much needed distractions throughout this degree, thank you for my sanity. And possibly most important, I would like to thank and send my love to Davos, Gally, and Tess for their joy, silliness, and fluffy support.

Lastly, but most certainly not least, I would love to thank the friends I have made throughout this degree and my time here in Toronto. There are too many of you to list however know you all will never leave my heart or thoughts. Roommates, confidants, and nacho pals, you have all supported me endlessly, thank you. And Bill, that means you too. Thank you for supporting me and Amir since our arrival here, if it weren't for you I would never have continued through to complete a masters. You show far more kindness then you will ever admit.

Contents

Abstract	iii
Acknowledgements	iv
List of Tables	viii
List of Figures	ix
List of Appendices	xi
Nomenclature	xii
1 Introduction	1
1.1 Research Objectives	2
1.2 Thesis Structure	2
2 Background and Literature Review	4
2.1 Gust Energy Harvesting	4
2.1.1 Active Gust Energy Harvesting	6
2.1.2 Passive Gust Energy Harvesting	7
2.2 Aeroelastic Tailoring	8
2.3 Composite Wing Architecture	9
2.3.1 Composite Design	10
2.3.2 Fabrication Techniques	12
2.4 Modeling and Design of Composite Structures	13
3 Gust Energy Harvesting Model	15
3.1 Gust Energy Harvesting Efficiency Factor	16
3.2 Aeroelastic Model	18
4 Composite Structural Model	22

4.1	Equivalent Plate Model	22
4.2	Equivalent Plate and Classical Laminate Plate Theory	24
4.3	Equivalent Plate Method Validation	29
4.4	Wing Section Shear Center	35
5	Design Approach	37
5.1	Baseline Aircraft Evaluation	38
5.2	Design Optimization	39
5.2.1	Structural Optimization	40
5.2.2	Layup Selection	41
6	Results and Case Study	44
6.1	Baseline Aircraft Performance	47
6.2	Structural Optimization	50
6.3	Layup Selection	52
6.4	Proposed Aircraft Configuration Performance	56
7	Future Work and Development	60
7.1	Structural Testing	60
7.2	Flight Testing	61
8	Conclusion	63
Appendices		65
References		79

List of Tables

1	Required input parameters for selection model or optimization.	16
2	SW117 aircraft parameters.	44
3	Baseline aircraft sandwich structure.	46
4	Performance of optimized and segmented configurations.	51
5	Segmented composite layup at 3 spanwise locations.	54
6	Single composite layup selection.	54
7	Performance of baseline and final configurations.	56

List of Figures

1	a) Discrete sinusoidal gust profile, b) Discrete 1-cosine gust profile, c) Continuous gust profile	5
2	Gust affects on wingsection lift and drag response.	8
3	Sandwich composite structure.	12
4	Dynamic structural solution algorithm.	19
5	Initial structure (A), Equivalent plate (B).	23
6	Equivalent plate for a wing section.	24
7	Wing geometry and testing apparatus definition.	30
8	Comparison of equivalent plate model and experimental testing at DS2. .	33
9	Comparison of equivalent plate model and experimental testing at DS1. .	34
10	Structural idealization to find shear center for NACA0010.	35
11	Baseline aircraft evaluation process.	38
12	Optimized design selection process.	40
13	Solar powered UAS, “SW117”	44
14	Baseline aircraft cross-section and idealized structure for shear center evaluation. (<i>Scaled by undisclosed factor to protect proprietary information</i>) .	45
15	Equivalent plate reduction of baseline wing cross-section along the X-Z plane. (<i>not to scale</i>)	46
16	Energy altitude gains of SW117 aircraft passing through a sinusoidal gust.	48
17	Gust affects on wingtip deflection, twist, and energy altitude gains . . .	49
18	Wing panel structural configurations of wing halfspan. (<i>Not to scale</i>) . .	50
19	Achievable wing structural properties based on available composite materials and manufacturing constraints.	53
20	Bending and torsional rigidity structural element distribution for given half-span configuration.	55
21	3-Segment aircraft configuration performance within a gust.	57

22	Change in energy altitude for baseline and final segmented aircrafts within a discrete downward gust.	58
23	Proposed whiffletree configuration for structural testing.	61

Appendices

Appendix A Equivalent Plate Evaluation	65
Appendix B Idealized Shear Center Location	68
Figure B.1 NACA0010 Structural idealization	68
Figure B.2 Triangular moment arm for shear center evaluation for nodes 2 to 5	70
Appendix C Aeroelastic Model Input Example	71
Appendix D Optimized Aircraft Configuration	76
Table D.1 Optimized and segmented SW117 aircraft configurations	76
Appendix E Effects of Manufacturing Irregularities	77
Figure E.1 Sensitivity of manufacturing irregularities on structural parameters	77

Nomenclature

ΔD Change in drag.

ΔL Change in lift.

α_{eff} Effective angle of attack.

L_o Cruise lift.

W_g Vertical gust magnitude.

V_{inf} Freestream velocity.

ΔE_g Energy change through a gust.

AR Aspect ratio.

α Angle of attack.

S Wingspan.

L_g Gust length.

e Span efficiency.

z_e Energy altitude.

z Altitude.

η Gust harvesting efficiency.

y_{tip} Wingtip deflection.

EI Bending stiffness.

GJ Torsional rigidity.

a Bending beam point load location.

f_1 Natural frequency.

m Mass.

LM Beam mass per unit length.

I_{xx} Area moment of inertia.

- A Component area.
- E_x Yonge's modulus.
- ν Poisson's ratio.
- f Fabric-to-resin ratio.
- Q Stiffness matrix.
- \bar{Q} Reduced stiffness matrix.
- B Idealized boom area.
- y_j Location of node j from X-axis.
- t Thickness.
- G Shear modulus.
- P_{gust} Power extracted from gust.
- t_{gust} Time spent within gust.
- W Parameter scoring weighting.

1 Introduction

This thesis presents a method to reduce the net power draw on an aircraft through gust energy harvesting and structural design, with a primary focus on reducing the net power draw for unmanned aerial systems, *UAS*. Gust energy harvesting is a process that involves the design of aircraft structures [1–5], mechanisms [6–8], and flight paths [9] that support the active or passive extraction of energy from a gusty environment. Gusts, characterized by a lateral (horizontal) or vertical air-mass motion, may vary in magnitude based on altitude, time of day, or environmental features such as cliffs and tree lines. The statistical range of expected gusts is well documented [10–12]; however, the actual experienced gusts throughout any operation will vary unpredictably [10]. To incorporate gust energy harvesting into the preliminary design stage of an aircraft, it is important to consider the possible penalties, such as additional weight. Composite materials have proven to serve as reliable and versatile materials that allow for the tailoring of a wing’s stiffness while minimizing the overall weight costs when compared to traditional isotropic materials [13, 14].

Aeroelastic tailoring is a design process that considers the interactions between an elastic structure and aerodynamic forces [15]. The aeroelastic tailoring of a composite wing, when considering gust energy harvesting, has been shown to be capable of achieving significant savings for high performance aircraft sailplanes [1–3]. Wing drag reductions of up to 10.5% [1, 4] have been predicted. Including gust energy harvesting through aeroelastic tailoring in the aircraft design process can reduce the required power.

The work completed in this thesis was made possible through the continued support of Superwake LTD, a UAS company based out of Toronto, Ontario. The work carried out in this thesis was used to select a composite wing structure for Superwake’s SW117 aircraft. The new composite wing structure was selected to increase the aircraft’s gust energy harvesting capabilities. The SW117 aircraft is discussed in more detail in Chapter 6.

1.1 Research Objectives

The study presented in the following sections aims to answer the following central and the subsequent secondary research questions:

What performance gains are possible through gust energy harvesting for a small, high-endurance, UAS using aeroelastic tailoring methods?

- What structural design parameters are most relevant when considering gust-energy harvesting?
- What fidelity of modeling is required to determine the influence of a composite layup schedule on the relevant structural parameters?
- What are the limitations of gust energy harvesting and how can an appropriate structural design space be selected?

1.2 Thesis Structure

Chapter 1 of this thesis introduces the research objectives that guided the research for the selection of a composite structure, selected through aeroelastic tailoring, to increase the gust energy harvesting potential of a baseline aircraft.

Chapter 2 outlines the relevant research into the fields of active and passive gust energy harvesting, aeroelastic tailoring, and composite wing design and modeling. An aeroelastic tailoring model is introduced that was developed by Melville [1] and was used to select an optimized wing structure.

Chapter 3 further outlines gust energy harvesting and the aeroelastic model used to quantify the gust energy harvesting potential for a selected aircraft. The gust energy harvesting for a selected aircraft is quantified through the use of a gust energy harvesting factor that compares the simulated change in energy altitude for a given aircraft to the ideal maximum available energy within a gust.

Chapter 4 presents a low-fidelity method to quickly evaluate a wing through the representation of the wing as an equivalent plate. The equivalent plate model was used to allow for classical laminate plate theory to be used to evaluate the structural behavior of a composite wing and was compared to existing experimental data.

Chapter 5 discusses the design approach that applies the aeroelastic and composite models and uses a genetic algorithm to select an optimized wing structure. The presented design approach outlines a method that evaluates a baseline aircraft's performance, determines an optimized structure configuration, and selects a composite structure that satisfies the optimized structure.

Chapter 6 outlines the application of the presented design approach when considering a chosen baseline aircraft configuration. A structural design space is defined based on the available composite materials and selected manufacturing constraints which is used for the selection of a composite wing structure that satisfies the optimized structure. Multiple structural configurations are proposed based on the defined constraints and the performance gains for each design are compared to allow for the selection of a design that extracts more energy from a turbulent atmosphere.

Chapter 7 discusses the future work required to develop and test the optimized aeroelastically tailored design.

2 Background and Literature Review

Gust harvesting has demonstrated potential for energy savings [1–4]; to maximize these savings aeroelastic tailoring need to be included in the preliminary design stage of an aircraft. This chapter reviews existing studies on the applications of gust harvesting and explores the potential drag reductions available through aeroelastic tailoring. The discussion on potential energy savings outlines composite wing design and modeling methods aimed at establishing a reliable yet computationally efficient process for integrating aeroelastics into the design of composite aircraft. In addition, in this chapter composite wing-design and modeling techniques are discussed that support an efficient, yet reliable process for integrating aeroelastic considerations into aircraft design.

2.1 Gust Energy Harvesting

Throughout the operation of an aircraft lateral and vertical gusts are encountered in varying magnitudes [10,11]. These gusts have the potential for energy gains through gust harvesting. Gust harvesting can take the form of active or passive energy harvesting. For this study only vertical gusts are considered as these gusts have the greatest effect on the loading experienced by the aircraft [16]; however, the available gains from lateral gusts is discussed in Section 2.1.1.1 for completeness. The vertical gust limit load cases outlined in FAR25 require an aircraft to be designed for a discrete gust load of up to a maximum of 50ft/s or 17m/s while operating below 15,000ft [11]. However, a study completed by the Australian Department of Defense [10] suggests that these values are overly conservative, and suggests a lesser likelihood of large magnitude gusts at low altitudes [10]. While the maximum vertical loading may be overestimated, operating at low altitudes increases the likelihood of encountering gusts due to ground effects and thermals [17]. The increased presence of turbulent air motion at altitudes lower than 15,000 ft results in greater gust harvesting potential.

Figure 1, shows three gust models: a sinusoidal gust and 1-cosine gusts that are examples of discrete gusts, and a von-Karman profile that is an example of a continuous gust. Continuous gusts are generally based on statistical data to replicate the expected aerodynamic loading throughout the operation of an aircraft [10], allowing for a robust but computationally intensive simulation. In contrast to continuous gusts, discrete gusts require are simpler to evaluate computationally and have been shown to adequately capture the aeroelastic response of an aircraft and the aircraft's gust energy harvesting performance [1].

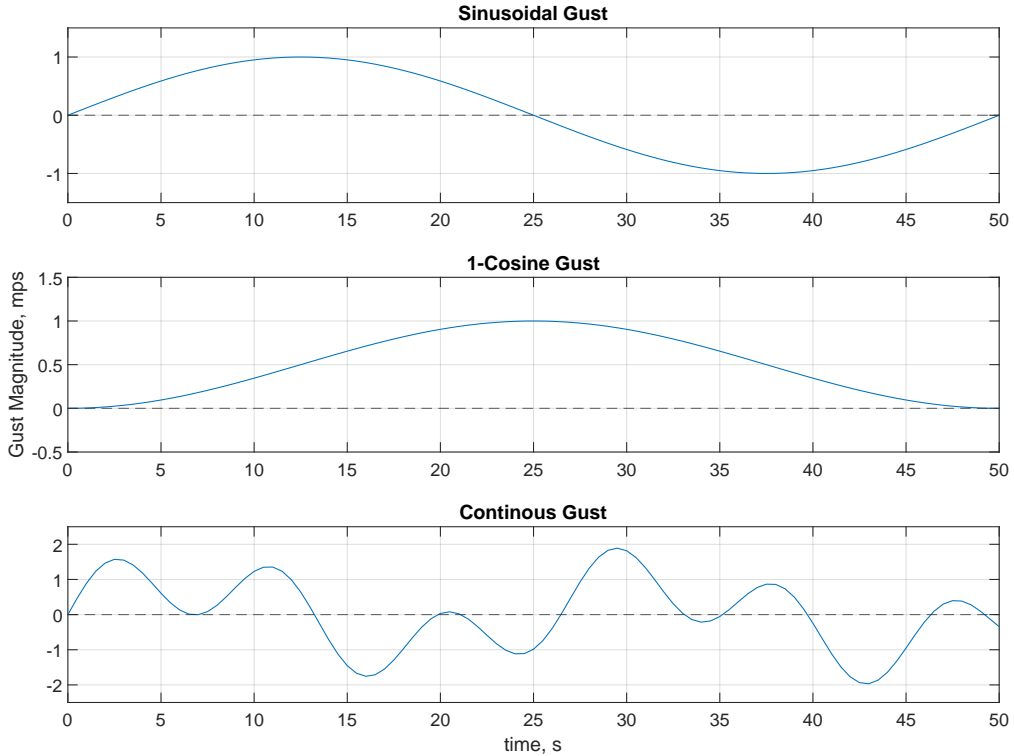


Figure 1: a) Discrete sinusoidal gust profile, b) Discrete 1-cosine gust profile, c) Continuous gust profile

Many profiles can be used to represent a discrete gust [18]; however, a sinusoidal gust profile has the highest value for this study due to their net-zero effect on the total motion of the airmass. The sinusoidal gust profile shown in Fig. 1 is an example of a gust that has a net-zero effect on the airmass, since there are equal positive and negative gust

effects when considering the gust as a whole. By evaluating a simulated aircraft that traverses a sinusoidal gust, an understanding of the possible net gains, or reduction in losses, can be shown and related to the uncertain day-to-day gust conditions experienced during regular operations [1, 8].

During a flight, thermalling and ridge soaring are examples of flight methods that take advantage of primarily positive vertical air motion available and are examples of active gust harvesting through flight path planning. In contrast to the net-positive scenario that the 1-cosine gust addresses, a von-Karman gust aims to model the possible behavior of a gusty environment throughout a set period. Von-Karman gusts allow for the simulation of a random, statistically possible continuous operation and allows for an increased understanding of the possible dynamic interactions of the wing when experiencing multiple, consecutive gusts. A combination of net-positive, net-zero, and continuous gusts allows for the behavior of the vehicle to be captured under a range of scenarios to simulate the performance changes of an aircraft within a turbulent atmosphere.

2.1.1 Active Gust Energy Harvesting

2.1.1.1 Dynamic Soaring

Dynamic soaring is an example of active gust energy harvesting, which takes advantage of wind gradients. Wind gradients are the result of the change in wind direction or intensity with an increase in altitude [5, 9]. Dynamic soaring requires regularly altering the flight path and an available method to monitor wind gradients. Energy can be extracted from horizontal gusts through the use of dynamic soaring flight path strategies. However, the flight path of the aircraft essentially becomes dependent on the wind, which can affect the range or operation of the vehicle, making realistic applications of dynamic soaring limited.

2.1.1.2 Gust Alleviation

Another method for approaching gust energy harvesting involves limiting structural loads during high gust loading. The use of control surface [19] is an example of active gust alleviation. By actively reducing the maximum gust loading experienced by the aircraft, the structural weight can be reduced. Other methods have been proposed, such as the use of micro-tabs, that reduce the drag increase by comparison to the aerodynamic drag resulting from flap deflection [6].

2.1.2 Passive Gust Energy Harvesting

Passive gust energy harvesting involves the application of design methodologies that do not require active inputs to the aircraft or additional power draw. The passive gust energy harvesting methods presented have the potential to extract energy from the atmosphere across a wider range of conditions due to the continuous nature of the energy harvesting methods. The passive methods presented allow for energy savings while within a wide range of positive and negative gusts minimizing the situational constraints often encountered with many active gust energy harvesting techniques. At the cost of increased design and manufacturing complexity, passive gust harvesting has the potential to reduce the expected power draw throughout the operation of an aircraft.

2.1.2.1 Piezoelectric Structures

One example of a passive gust harvesting method is the use of piezoelectric composite materials in manufacturing a flexible wing. Piezoelectric materials allow for electrical power to be generated through the deflections experienced by a wing [7, 20]. By including a piezoelectric composite material in the skin or spar of the wing, a current can be drawn from the structure and used as electrical power for onboard batteries. During wind tunnel testing gains were shown to be minor, around 0.188 mW [7]. The manufacturing and design complexity of adding piezoelectric structures is significant due to the mate-

rial placement limitations enforced by communication interference or other conductive materials in contact with the structures.

2.1.2.2 Gust Energy Harvesting through Structural Dynamics

Figure 2 shows an example of a rigid wing encountering a vertical gust, where the increased effective angle of attack results in the lift vector being tilted forward thus projecting a thrust component in the general flight direction. $-\Delta D$. The drag reductions due to an upward gust are larger compared to the drag increases due to an equivalent downward gust, shown in Fig.2b. It is smaller than the drag reduction of the upward gust due to the reduction in effective angle of attack. Thus, a net-drag reduction can be demonstrated despite net-zero air-mass motion. The energy transfer from gust to wing and subsequent drag reduction can be improved using certain structural-dynamic properties for the wing, in particular the wing bending-torsion coupling [1].

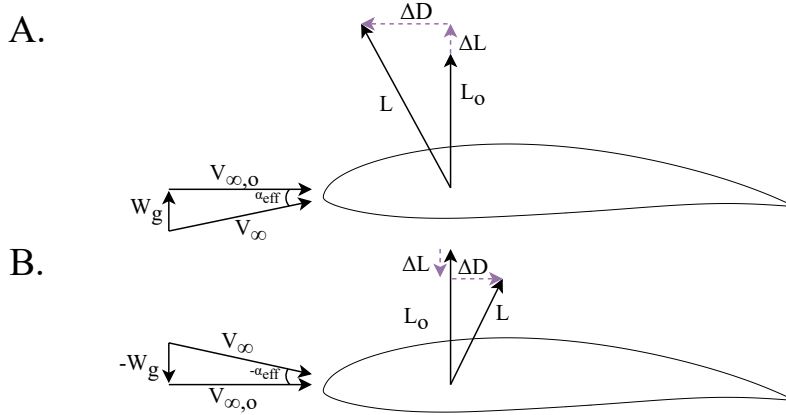


Figure 2: Gust affects on wingsection lift and drag response in: a) vertical gust, b) downward gust [2].

2.2 Aeroelastic Tailoring

Passive gust energy harvesting has been shown to reduce the wing drag up to 10.5% purely through aeroelastic tailoring of the wing structure [1, 4]. This value is, among other aspects, a function of gust strength. To model this drag reduction an analysis tool

was proposed by Melville [1] that captures the dynamic response of an elastic structure through the combination of a coupled bending-torsion Euler-Bernoulli beam model and a higher-order potential flow model. Respectively, the presented tool captures the structural and aerodynamic response of an elastic wing with a rigid fuselage and tail structure. Melville [1] found good agreement between the proposed tool and existing literature; the proposed tool was used to quantify the effects of bending stiffness, torsional rigidity, and the shear center placement on the gust energy harvesting potential for an aircraft. A comprehensive exploration of the discussed method and tool is outlined in Chapter 3.

The study completed by Melville [1] found that increasing the bending stiffness and reducing the torsional rigidity allowed for an increase in the gust energy harvesting potential for an aircraft. The shear center placement, with respect to the center of gravity, was shown to have minor effects on the energy harvesting. The study was able to show that alterations to structural parameters resulted in a 12% reduction in sink rate while within a sinusoidal gust with a maximum amplitude of 1 m/s by comparison to the scenario without a gust [1].

2.3 Composite Wing Architecture

Composite structures provide unique design opportunities for aeroelastic tailored aircraft as the orientation of the fabrics can be selected to support varying or constant spanwise stiffness parameters, allowing for increased control over the structural response of the aircraft [14]. The preliminary design of an aircraft's wingbox to take advantage of gust energy harvesting through aeroelastic tailoring allows for a structure to be selected and manufactured that takes advantage of the energy available within a turbulent atmosphere. A standard wingbox can be broken into the primary and rear spar component along with the upper and lower skin surfaces [21] in order to approximate the aircraft structure. A wing skin and spar cap layup can be selected to achieve the desired structural properties before stiffeners, ribs, and other detailed designs are included in future

design stages. A low-fidelity model can effectively aid in selecting a composite wing layup by limiting the computational costs associated with considering gust harvesting in the structural design phase.

Composite materials allow for increased control over structural parameters and, most importantly, the ability to decrease the weight penalties required to achieve the same strengths. The selection of a composite layup can be a computational intense process with a wide range of modeling accuracies [22]. To incorporate gust harvesting during the preliminary design stage of a composite wing structure, a low-fidelity, low-computation cost solution allows for a quick and efficient method of selecting an acceptable layup. The varying fidelity and benefits of different composite wing models will be discussed in Section 2.4.

2.3.1 Composite Design

In this study, the selection of the primary composite structures for a wing structure is discussed. The wing skin, spars, and supporting elements such as ribs and stiffeners are all examples of primary wing structures. The wing skin and spars have the most significant effect on the overall stiffness of a wing; where the wing skin provides torsional stiffness and a smooth aerodynamic surface, and the spars provide bending rigidity through the spar caps. The primary purpose of ribs and stiffeners is to maintain the wing's geometry across the span and to prevent buckling in the skin.

A typical composite material spar is comprised of spar caps, flanges and a web. Spar caps serve as the primary source of bending stiffness for a wing and are generally made of a couple of layers of unidirectional fibers. The spar itself is made of a web that provides stiffness to the spar structure and can take the form of multiple composite layers or a low-strength and stiffness foam material constrained by two outer fabric layers. The flanges serve as a bonding location between the skin and the spar and fillets to reduce stress concentrations and local splitting or delamination. Finally, an outer layer of fabric is used to hold the entire structure together. In the case of multiple spars being used,

the section between the rearmost and front-most spars can be considered the wingbox, as this location provides the largest stiffness across the wing. A wingbox analysis is outlined in Section 2.4 and in Chapter 3.

The wing skin provides the primary source of torsional stiffness and serves as a method to transferring the aerodynamic loads to the ribs and spars. Due to the skin providing the central torsional stiffness for an aircraft, the skin serves as the primary design consideration when considering gust harvesting through aeroelastic tailoring. The wing skin of a composite aircraft can take the form of a monolithic layup featuring only composite laminate or a sandwich layup that features two or more layers of structural fabric bonded to the external surfaces of a low-strength for, core material to increase the inertia of the structure.

Monolithic Composite Various fabrics can be used when designing a composite layup, including fiberglass, carbon fibers, and aramid fibers; if a composite layup is purely comprised of these structural fabrics, it is considered a monolithic layup. The benefit of monolithic layups is the tightly packed tensile strength, providing high tensile strength with a minimal thickness; however, the lack of thickness results in low bending rigidity and susceptibility to buckling. A sandwich composite can be used to achieve a higher bending stiffness without the introduction of an unreasonable amount of fabric layers, resulting in high weights and cost.

Sandwich Composite Sandwich composites are particularly suitable for wing skins due to their resistance to buckling and puncturing during handling while providing the desired bending stiffness. This is achieved without the additional weight and cost associated with the numerous layers required to attain the same performance with a monolithic structure. A sandwich composite, as shown in Fig. 3, features a low-strength core material that provides an increase in the skin's moment of inertia and is sandwiched between two composite material facesheets. These facesheets provide the primary strength for the

structure. The overall weight and cost of the structure can be reduced by reducing the number of composite fabric layers compared to a monolithic composite.

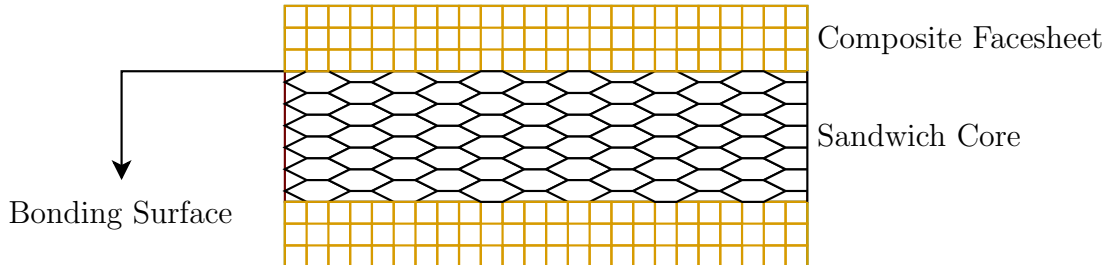


Figure 3: Sandwich composite structure [21].

2.3.2 Fabrication Techniques

Wet layups, pre-preg layups, and resin infusion are all examples of composite fabrication techniques. The manufacturing of a composite structure requires the matrix to be incorporated into the composite fabric. Wet layups are a manufacturing technique that is largely completed manually, and are used primarily for their simplicity [23]. The simplicity of the wet layup results in a variety of drawbacks including fiber alignment issues, lack of control over the fiber-volume ratio, and difficulty avoiding voids. Pre-preg and resin infusion techniques address these concerns. Pre-preg layups use a material that has an uncured matrix material and requires a specific combination of temperature and pressure to cure. Pre-preg layups allow for good control over the fiber-volume ratio due to the material coming from a supplier with a specified ratio. However, pre-preg layups require temperature and humidity controlled environments to prevent undesired curing or moisture retention, as well as a method to cure the material such as an autoclave [23]. Resin infusion fabrication techniques use dry fabrics that are injected with resin allowing for good surface finish, manufacturing repeatability, and this process does not require an autoclave. Resin infusion is highly reliant on the surface finish of product molds and therefore requires high upfront cost to manufacture and then maintain the molds. Similar to pre-preg layups, resin infusion allows for consistent fiber-volume ratios. Resin infusion is the primary composite fabrication technique suggested for the work of this thesis.

2.4 Modeling and Design of Composite Structures

The modeling of a composite wing takes the form of low-fidelity estimations through hand calculations, or high-fidelity modeling such as finite element methods. The selection of an appropriate model is dependent on the balance between the resolution and accuracy of the model, and the modeling costs through time, computational effort, and program licenses. The selection of a low-fidelity model comes with many limitations that define under what circumstances the method can be used while maintaining an acceptable level of real-world accuracy. However, selecting a high-fidelity model comes at the cost of experienced modeling time to ensure the model created represents the real world. This section outlines a couple of low-fidelity and high-fidelity models that can be used and their associated possibilities and limitations. The selected models is further explored in Chapter 3.

A finite element method for modeling the development of a composite aircraft from coupon testing to the aircraft simulation stage is discussed in Pogosyan et al. [24]. This article highlights the importance of multidisciplinary research that combines the aerodynamic, structural, and composite calculations required to develop a comprehensive airframe that reliably simulates the desired airframe under expected loading. Before beginning the design and development of a composite aircraft through finite element analysis, the material must be characterized in the coupon investigation. Pogosyan et al. [24] discussed the homogenization of the smallest representative portions of the modeled material, also known as representative volume elements. The modeling of a coupon test provides for the integration of other failure modes to be tested, such as delamination or buckling within the model. After evaluating the composite model's material properties and behaviors, the larger structural and aerodynamic models can be applied during wing and airframe design. The modeling of a composite structure through finite element analysis allows for many failure modes to be investigated during the design stages. However, the computational cost is high, and the mischaracterization of the initial materials and

behaviors can result in inaccurate results.

A low-fidelity equivalent plate model is proposed by Kilimtzidis et al. [25] that aims to achieve an efficient modeling method for the early aircraft design of transport aircraft. The model's accuracy is compared to finite element models created in NASTRAN to show good agreement of, on average, 2.77% in the eigenfrequencies. The proposed method estimates that a wing behaves like a flat plate and requires a large chord-to-thickness ratio and a low camber to satisfy this condition. By modeling the wing as a flat plate and sectioning the wing across the span, the computational effort required was reduced from hours to seconds. The limitations associated with applying the equivalent plate method include limitations on the airfoil thickness and camber and the lack of insight into other failure modes that higher fidelity models, such as finite elements methods, can capture. Failure modes such as buckling and delamination must be evaluated in addition to the purely structural model resulting from the equivalent plate method.

When modeling composite aircraft, an appropriate method must be selected to satisfy the design requirements and the computational or time constraints. High-fidelity models, such as those proposed by Pogosyan et al. [24], capture many failure criteria with limited structural assumptions, resulting in a high order of confidence in the final results. However, the modeling process is intensive and expensive through time-on-task and program licenses. Should a designer require quick and cheap modeling of a thin and low-camber airfoil, the application of a model similar to the equivalent plate model applied by Kilimtzidis et al. [25] and documented in Giles et al. [26], can be used. To include aeroelastic tailoring in the design process of a composite aircraft, the changes to the layup structure need to be made before the detailed aircraft design stages, and therefore, the application of a low-fidelity composite model would allow for simple and reliable results that can be iterated on so long as the aircraft design space satisfies the limitations defined by the modeling method.

3 Gust Energy Harvesting Model

An aeroelastic tailoring method proposed by Melville [1] is applied and explored in the following section to evaluate an aircraft's ability to extract energy from a turbulent atmosphere. The selected method simulates an aircraft traversing a prescribed gust profile, as outlined in Section 2.1, and evaluates the elastic-structural response. The simulated aircraft maintains a fixed-stick flight condition resulting in the motion of the aircraft being purely a result of the simulated flight conditions and the aircraft's dynamic response. The gust energy harvesting, structural, and composite models and methods outlined in Chapter 3 and 4 are utilized alongside the discussed aeroelastic tailoring method to select a composite structure that gains more energy while traversing a gust. The application of the models and methods shown in Table 1 for the selection of a new wing structure are discussed in Chapter 5. The models and methods shown in Table 1 are outlined in Chapters 3 and 4.

Table 1, shows the required input parameters for the models and optimization processes in structural design approach. The checkmarks represent the input parameters needed to evaluate the desired process. In contrast, the o symbol represents a parameter that is an output used by a process that appears later in the design approach. The processes are presented in the prescribed order of completion, from left to right, where the far left processes represent the model of the baseline aircraft, and the far right processes represent the selection of the final proposed design. Before aeroelastic tailoring can be considered and the adequate savings quantified, the inputs for the baseline aircraft, outlined in Table 1, must be provided.

Table 1: Required input parameters for selection model or optimization.

Parameters	Quantify Gust Harvesting Potential	Aeroelastic, Structural Model	Aeroelastic, Aerodynamic Model	Structural Optimization for Gust Harvesting	Equivalent Plate Model	Layup Selection Parameter Sweep	Layup Scoring and Selection Metrics
Wing Geometry	✓	-	-	-	-	-	-
Wing Cross-Section	-	✓	✓	-	✓	-	-
Aircraft Weight Breakdown	✓	✓	✓	✓	-	-	-
Design Load Case(s)	✓	✓	-	✓	-	-	-
Cruise Conditions	✓	-	✓	✓	-	-	-
Baseline Aircraft Configuration	✓	✓	✓	✓	-	-	-
Baseline Aircraft Performance	-	o	o	✓	-	-	-
Composite Database	-	-	-	-	-	✓	✓
Manufacturing Constraints	-	-	-	-	-	✓	✓

✓ Require input parameter for selected model or process.

o Output parameter from selected model or process.

3.1 Gust Energy Harvesting Efficiency Factor

To describe the energy available within a vertical gust and the ability of various aircraft to extract energy from said environment, a gust-efficiency factor can be used to quantify the maximum energy that can be extracted. The energy available within a vertical gust for a rigid aircraft that moves along a linear flight path can be defined using the following [3]:

$$\Delta E_g = \int_0^{L_g} qSa \left(\alpha \Delta \alpha \left(1 - \frac{2a}{\pi A Re} \right) + (\Delta \alpha)^2 \left(1 - \frac{a}{\pi A Re} \right) \right) dx \quad (1)$$

where the energy is a factor of the aspect ratio, AR , the span efficiency, e , the lift curve slope, a , and the angle of attack and its change through the gust, α [3]. The energy change seen can be expressed as an energy altitude, z_e , that represents the combined energy state of the vehicle as an effective altitude,

$$\Delta z_{e,ideal} = \frac{\Delta E_g}{mg} \quad (2)$$

where m is the mass of the aircraft and g is the gravitational constant. The maximum ideal energy altitude, in meters, can be compared to the measured change in energy altitude of an aircraft by through the definition of the initial and finally state of the vehicle,

$$\Delta z_e = \frac{1}{2g}(U_f^2 - U_0^2) + (z_f - z_0) \quad (3)$$

where U_0 and U_f are the airspeeds at beginning and end of the time interval in-question. z_0 and z_f are the respective altitudes. The two states of the vehicle can either be found through experimental testing or through the application of a simulated aircraft. The relationship between the actual energy extracted while traversing a gust by comparison to the theoretical value of Eq. 2 is,

$$\eta = \frac{\Delta z_e}{\Delta z_{e,ideal}} \quad (4)$$

The maximum theoretical energy, ΔE_g , describes the potential energy gain while traversing a prescribed gust. The idealized gains may be small for the given aircraft, resulting in fundamental changes to the design should gust harvesting be desired. To increase the gust harvesting potential of an aircraft, it was shown that decreasing the span loading and increasing the span efficiency, the wing span, and the aspect ratio of the wing will result in higher potential gains [3]. Before gust harvesting can be included as a consideration for a vehicle, the relative achievable savings must be considered.

The change in energy experienced through a gust is related to power savings based on the change in energy over the time spent in the gust, allowing for the gust harvesting savings to be directly compared to the aerodynamic power required. The energy altitude change across the prescribed gust, represented as Δz_e , may be related to a reduction in aerodynamic power draw.

$$\Delta E_{gust} = \Delta z_e mg \quad (5)$$

$$\bar{P}_{gust} = \frac{\Delta z_e \cdot mg}{t_{gust}} \quad (6)$$

When considering aeroelastic tailoring, the average power reduction required, P_{gust} , depends on the change in energy altitude across the gust and the amount of time spent within the gust. It is important to note that while the analysis presented in this work focuses on a study of a single discrete gust. The parameter, Δz_e , represents the summation of the change in energy altitude and is used to evaluate the average power savings experienced. For this evaluation the energy altitude change, shown in Eq. 3, is used to quantify the net change in the aircraft's energy state across the length of the gust. The average power reduction across the gust, which is related to the energy altitude of the aircraft in Eq. 6, can be compared to the total power required.

3.2 Aeroelastic Model

The aeroelastic model proposed by Melville [1] simulates the dynamic response of an elastic wing structure and otherwise rigid airframe that traverse a defined gust profile. The model evaluates the response of the elastic wing using an Euler-Bernoulli beam model for the structural response of the wing and a higher-order potential lifting surface method for the aerodynamic loading. A simple stick-fixed flight dynamics model captures the flight trajectory of the simulated aircraft.

Structural Model

The coupling of the aerodynamic and the structural model allows for the dynamic response of the aircraft to be evaluated [1, 27]. The beam method selected evaluates the wing's bending and torsional response along with the bending-twist coupling resulting from the non-zero distance between the center of gravity and the elastic axis, the position locus of the chordwise shear center locations. The coupling from the structural geometry is captured through the displacement between the center of gravity and the shear center. The Euler-Bernoulli beam method allows for fast evaluation of the structural simulation while still capturing the bending, twisting, and internal coupling.

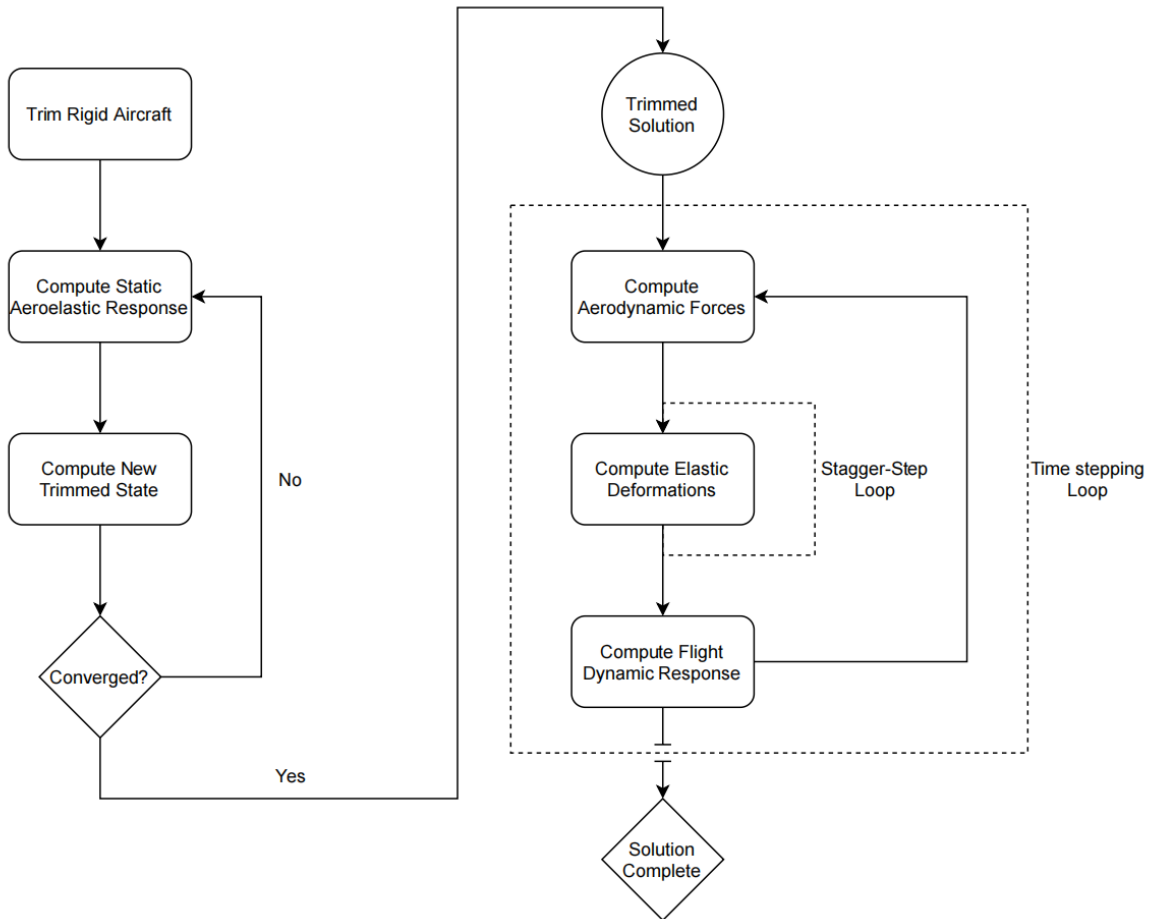


Figure 4: Dynamic structural solution algorithm [1].

The simulation of the structural response of the vehicle is solved through the process shown in Fig. 4. Prior to *time stepping loop* that simulates the response of the aircraft an initial trimmed solution for the aircraft is evaluated. The evaluation of the trimmed solution computes the aerodynamic loads and the trim condition required to achieve steady flight. To determine the structural response, the aerodynamic loads are related to the elastic deformations, allowing for the motion of the aircraft and the aircraft structures to be evaluated for each step. The structural solution evaluates the motion of the fuselage and tail resulting from the elastic forces from the wing and the aerodynamic loading of the horizontal stabilizer, while the wing is evaluated under the inertial, elastic, and aerodynamic loads. The elastic forces are evaluated through the application of a stagger-step method that solves multiple structural solutions at a small time step before updating the aerodynamic forces [1].

The aeroelastic model of Melville allows for evaluating the elastic response of aircraft structures under various unsteady aerodynamic loading [1]. By simulating an aircraft within a discrete gust, the aeroelastic model is used to evaluate the initial gust harvesting performance of a preliminary aircraft design, allowing for further design optimization.

Aerodynamic Model

To model a lifting surface, the span of the desired wing is broken into chordwise and spanwise elements that determine the resolution and the computation time of the analysis [1, 28]. The spanwise elements run from the leading edge to the trailing edge and are shed as distributed vorticity elements into the wake [28]. The circulation, resulting from the vorticity elements, is integrated across the wing section to solve for the resultant lift forces. The induced drag experienced by the simulated wing is evaluated along the trailing edge [28]. The profile drag only experiences minor changes when experiencing gust loading, and therefore, capturing the induced drag is vital to ensure the accuracy of the results. The aerodynamic model captures unsteady effects such as apparent mass effects [29].

A sensitivity study was completed as recommended by Melville [1] to evaluate the required grid element distribution for a specific aircraft to ensure the wing section and spanwise circulation distributions are captured specifically. The study's goal was to determine the minimum number of elements to adequately capture the aircraft's response and minimize the required computation time. Additionally, the aerodynamic model utilized does not capture the stall behavior of the wing and therefore the simulation of the aircraft must be limited to operating within the low-drag region of the aircraft.

4 Composite Structural Model

To evaluate an existing aircraft's wingbox for input into the aeroelastic model an estimation of the selected wing's structural parameters is required. As outlined in Table 1, the estimated equivalent structural parameters are needed to model the gust energy harvesting effectiveness of a provided aircraft. To evaluate the structural response of a composite wing, high-fidelity models such as finite element analysis can be used; however, to estimate the equivalent structure, a low-fidelity model can be used to reduce the computational costs. For the proposed method, an equivalent plate model is used to estimate an existing aircraft for the described case study and to select a new composite layup schedule for the new proposed design outlined in Chapter 5. A low-fidelity model was selected to evaluate multiple design in the parametric sweep, and the ability to solve thousands of cases in seconds allows for faster turn around times while still capturing the structural parameters.

4.1 Equivalent Plate Model

To evaluate an existing wing section, the structures can related to an equivalent plate for fast computation speeds. An equivalent plate is comprised of a stack of equal-thickness structural layers that are related to the initial structure by maintaining the mass moment of inertia of each individual layer [30]. An example is presented in Fig. 5 where the cross-hatched and the hatched structures are reduced to equal-width flat plates in addition to the initial dashed structure. By reducing the structure to an equivalent plate, the effects of each individual layer are preserved, allowing for the application of classical plate theory.

Table 1, presented at the beginning of this chapter, shows that only the geometry of the wing-cross section and the overall wing geometry is required to reduce the wing section to an equivalent plate. The wing planform is required in the case of a non-rectangular wing as each section of the wing is reduced independently.

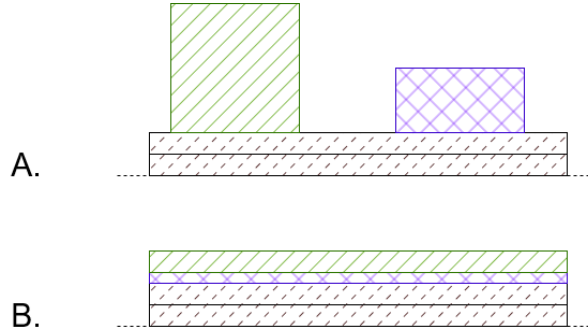


Figure 5: Initial structure (A), Equivalent plate (B).

To apply the equivalent plate method for a wing section, the wing skin, spar caps, and the spar web(s) must all be considered. To represent the wing section as a plate the area moment of inertia must be maintained between the two models for each layer. To do so the inertia, I_{xx} , of each layer is calculated,

$$I_{xx} = \int \int y^2 DA = I_{xxo} + Ay^2 \quad (7)$$

$$I_{yy} = \int \int x^2 DA = I_{yyo} + Ax^2 \quad (8)$$

where x and y define the location of the component and A is the cross sectional area. The moment of inertia must be maintained in the x and y directions to ensure bending and torsion analysis is correct. When modeling a wing section, that contains a large empty section in the center, an empty zone can be included in the equivalent plate to increase the moment of inertia of all material layers. To select an appropriate starting layer height for the inner wing the moment of inertia in the y-direction, I_{yy} , is solved for first, constraining the layer height and the placement of the plate is constrained by the moment of inertia along the x-axis. An example of an equivalent plate evaluation is outlined in Appendix A, and is seen in the case study in Chapter 5. By reducing a wing section into an equivalent plate, classical plate theory can be used.

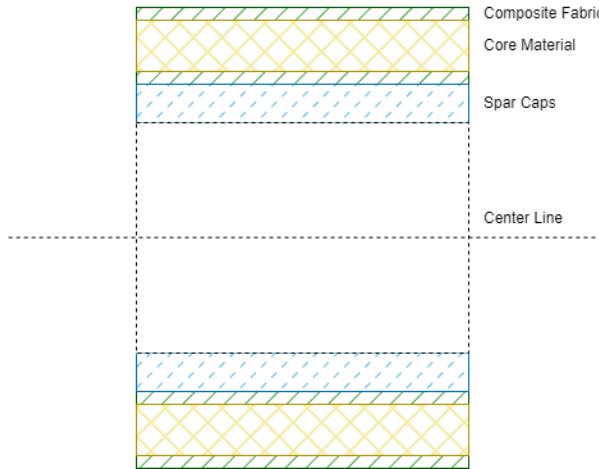


Figure 6: Equivalent plate for a wing section.

4.2 Equivalent Plate and Classical Laminate Plate Theory

By reducing a composite wing section into an equivalent plate, classical plate theory can be used to evaluate the bending and torsion stiffness of the desired wing structure. Classical plate theory allows for low computational cost solutions for a plate's stiffness and inertia parameters. Each layer of the composite laminate is evaluated based on the initial, dry fabric properties that can be found in composite databases such as MatWeb [31]. Below is an example of a database entry to be used with classical plate theory:

$$E_x = 245GPa, E_y = 245GPa, E_s = 20GPa, \nu = 0.3$$

The material properties presented are for a carbon fiber spread tow weave, therefore resulting in equal E_x and E_y elastic modulus'. To apply the dry material properties of a given fabric, the fiber-volume fraction needs to be known to describe the ratio of structural matrix to fibers. In the case of this study, epoxy resins will be used as the structural matrix for simplicity. However, other matrix materials that require varying manufacturing techniques exist, such as thermoplastics [32]. The fiber-volume fraction, v_f , of a material, is determined by knowing the volume of structural fabrics and matrix combined in the final composite part. Section 2.3.2 outlines a variety of composite manufacturing methods however for the analysis presented in this thesis resin infusion will be

used. Resin infusion was chosen as it is the composite manufacturing method of choice for Superwake. Through the measurement of the composite fabric, consumable materials, epoxy resin, and the final component weights a 0.55 fabric-to-resin ratio was found using,

$$v_f = \frac{M_f/\rho_f}{M_f/\rho_f + M_m/\rho_m} \quad (9)$$

The masses, M , of the fabric and the matrix are determined through the weighing of the initial materials and the final component and composite materials to determine the weight of the resin within the part. The densities, ρ , of the fabric and the matrix are based on published manufacture's data and the volume of the voids is assumed to be zero. Resin infusion is utilized in the manufacturing of the aircraft used in the case study in Chapter 6, and allows for consistent, and repeatable final parts with good consistency in both fiber-volume fraction and layer thickness. To include the resin and fabric properties in the initial layer properties, the rule of mixtures is applied to predict the structural properties of the composite laminate. The rule of mixtures conservatively estimates the shear modulus, G , or the elastic moduli, E , for the composite using,

$$P = \frac{P_m(1 + \zeta\psi v_f)}{1 - \psi v_f}, \text{ where } \psi = \frac{P_f - P_m}{P_f + \zeta P_m} \quad (10)$$

The properties of interest (P) are evaluated using ζ as 1 or 2 to find the shear modulus or the elastic modulus, respectively. With the layer properties determined, the stiffness matrix of each layer can be evaluated. The reduced stiffness matrix Q can be written,

$$Q = \begin{bmatrix} Q_{11} & Q_{12} & 0 \\ Q_{12} & Q_{22} & 0 \\ 0 & 0 & Q_{66} \end{bmatrix} \quad (11)$$

where the components of Q are,

$$\begin{aligned} Q_{11} &= m \cdot E_1 \\ Q_{22} &= m \cdot E_2 \\ Q_{12} &= m \cdot \nu_1 \cdot E_2 \\ Q_{66} &= E_s \end{aligned} \tag{12}$$

and where,

$$m = (1 - \nu_1 \nu_2)^{-1}$$

In the case of a [0/90] weave the material will have equal E_1 and E_2 stiffness values until the material is transformed into the loading frame. The material properties are shown with a ‘1’ along the fibers, and ‘2’ transverse to the fibers. The aerodynamic frame, or the loading frame, is shown with an ‘x’ in the flow direction, and ‘y’ across the span. Due to the materials all being weaves, each layer represents two orientations of fabric that are perpendicular to one-another, such as [0/90], [-45/45], or [-30/60]. The rotated reduced stiffness, \bar{Q} , in the aerodynamic frame, can be used to find the stress as a function of strain,

$$\begin{bmatrix} \sigma_x \\ \sigma_y \\ \tau_{xy} \end{bmatrix} = \begin{bmatrix} \bar{Q}_{xx} & \bar{Q}_{xy} & \bar{Q}_{xs} \\ \bar{Q}_{xy} & \bar{Q}_{yy} & \bar{Q}_{ys} \\ \bar{Q}_{xs} & \bar{Q}_{ys} & \bar{Q}_{ss} \end{bmatrix} \begin{bmatrix} \epsilon_x \\ \epsilon_y \\ \gamma_{xy} \end{bmatrix} \tag{13}$$

where the components of \bar{Q} are,

$$\begin{aligned}
\bar{Q}_{xx} &= Q_{11}m^4 + 2(Q_{12} + 2Q_{66})m^2n^2 + Q_{22}n^4 \\
\bar{Q}_{yy} &= Q_{11}n^4 + 2(Q_{12} + 2Q_{66})m^2n^2 + Q_{22}m^4 \\
\bar{Q}_{ss} &= (Q_{11} + Q_{12} - 2Q_{12} - 2Q_{66})m^2n^2 + Q_{66}(m^4 + n^4) \\
\bar{Q}_{xy} &= (Q_{11} + Q_{22} - 4Q_{66})m^2n^2 + Q_{12}(m^4 + n^4) \\
\bar{Q}_{xs} &= (Q_{11} - Q_{12} - 2Q_{66})m^3n + (Q_{12} - Q_{22} + 2Q_{66})mn^3 \\
\bar{Q}_{ys} &= (Q_{11} - Q_{12} - 2Q_{66})n^3m + (Q_{12} - Q_{22} + 2Q_{66})nm^3
\end{aligned} \tag{14}$$

and where,

$$m = \cos(\theta)$$

$$n = \sin(\theta)$$

With each layer of the material represented in the aeroelastic frame, the bending and torsional stiffness can be evaluated. The stiffness of a laminate plate depends on each layer's location, represented by a Z-distance from the centerline and the individual stiffness of each layer.

The stiffness of a laminate plate can be found using,

$$D_{ij} = \frac{1}{3} \sum_{k=1}^n (Q_{ij})_k (z_k^3 - z_{k-1}^3) \tag{15}$$

where D_{ij} represents the elements of bending stiffness matrix for the equivalent plate based on the selected new distance values for the equivalent plate. By reducing a two-dimensional wing section to an equivalent plate and evaluating the estimated stiffness of the wing, a low-computation effort solution can be applied in the case where many solutions must be found simultaneously.

The stiffness matrix of the composite wing section can be used to determine the bending stiffness, EI , and the torsional rigidity, GJ of the plate,

$$\begin{aligned}[d] &= [D]^{-1} \\ EI &= \frac{w}{d_{11}} \\ GJ &= \frac{w}{d_{66}}\end{aligned}\tag{16}$$

the bending and torsional stiffness of the wing section serves as the structural inputs to the aeroelastic model that evaluates the equivalent laminate plate with a wingbox width of w .

Equation 14 shows that angles of 0 and 90 degrees will result in \bar{Q}_{ys} and \bar{Q}_{xs} being equal to zero, resulting in zero bending-twist coupling in Eq. 15 from the laminate properties. Similarly, in the case of a composite material with equal primary-axis, Q_{11} , and secondary-axis, Q_{22} , stiffness values, there will be no bending-twist coupling. In the case of the off-axis rotated stiffness values, \bar{Q}_{xs} and \bar{Q}_{ys} , are non-zero coupling will occur, resulting in the wingtips washing in if the off-axis values are negative and washing out if the off-axis values are positive. Taking advantage of the bending-twist coupling resulting from the laminate properties' negative off-axis values, causing the wingtips to experience a wash-in effect, will result in an increased effective angle of attack at the wingtip, increasing the energy gains available within a vertical gust. Altering the composite fabrics' orientation within a wing's structures can result in a larger effective angle of attack gains while within a gust.

4.3 Equivalent Plate Method Validation

A paper presented by Sullivan et al. outlines the structural testing of an ultralight UAV through the application of a whiffletree testing apparatus [33]; the deflections experienced by the aircraft while under resultant loading forces ranging from 0 to 1600lbf (7.1kN) were used to validate the use of an equivalent plate model to estimate the structural parameters of a wing section. The aircraft presented features a halfspan length of 202.5 inches, and a limit load case of 900 lb for each wing [33]. The selected aircraft has a wing structure similar to the aircraft presented in the case study, with a single layer of core material sandwiched between multiple layers of structural fabrics and a spar cap with either 96 or 126 layers of fabric for the upper and lower main spar caps. The deflections experienced by the aircraft are presented in Fig. 7 and compared to the deflections predicted by applying the equivalent plate method as an input to the aeroelastic structural model.

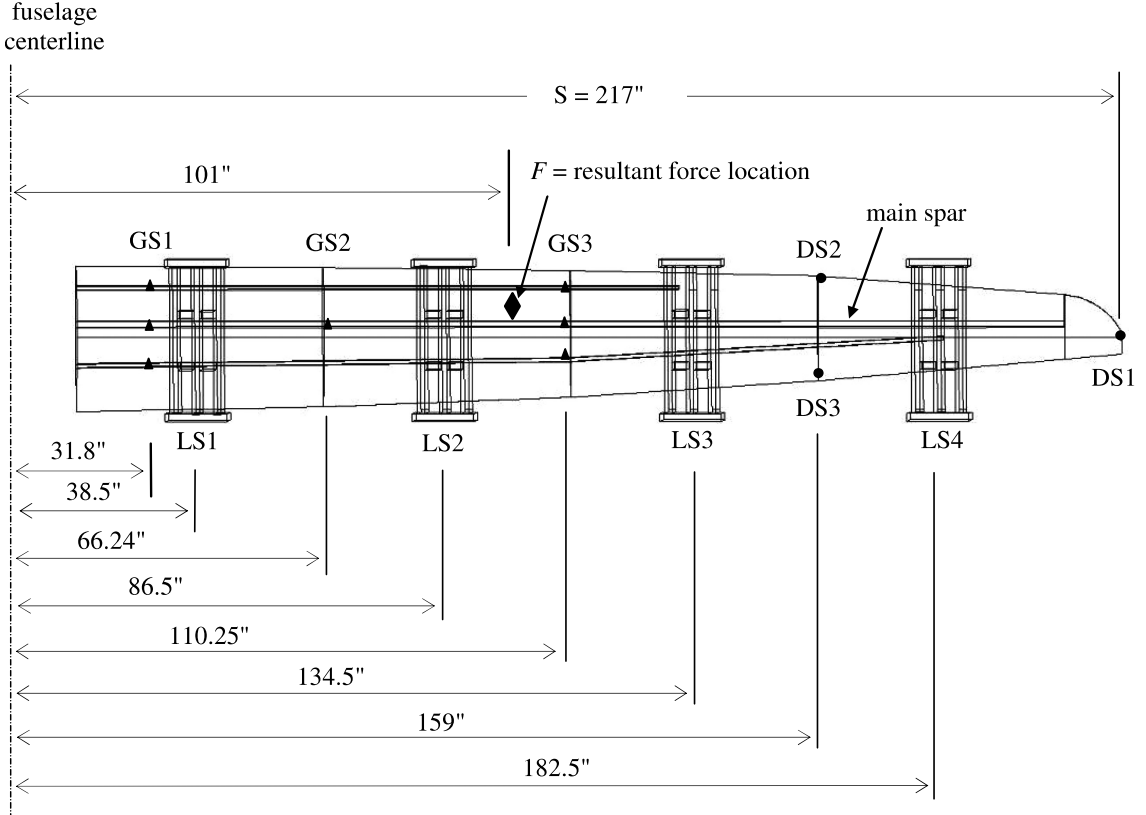


Figure 7: Wing geometry and testing apparatus definition [Reproduced from Ref. [33] with Permission].

The geometry of both the wing and whiffle tree support structures are shown in Fig.7 where LS1, LS2, LS3, and LS4 represent the support cradle structures. The features labeled as DS1, DS2 ,and DS3 represent locations where the deflections in the wing are measured using cable-extension deflection gauges. The present structure was estimated as an equivalent plate by evaluating the primary wing structures (spar caps and wing skin) at the beginning of all four wing panels and estimating the equivalent bending stiffness to calculate the deflections at DS2.

The EI for the four wing sections were evaluated through the use of the equivalent plate model and wing section geometry based on provided and estimate values through the use of ‘to-scale’ figures. The equivalent plate results assume a spar cap width of 1 inch and that the spar cap is located at a distance equal to 5% of the chord length from

the centerline. The spar cap values are estimated based on the to-scale figures provided in the material; however, the presented figure requires more information for comprehensive validation. The four separate wing sections shown in Fig.7 are determined to have bending stiffness values of:

$$EI_1 = 212 \text{ kN} \cdot \text{m}^2$$

$$EI_2 = 188 \text{ kN} \cdot \text{m}^2$$

$$EI_3 = 100 \text{ kN} \cdot \text{m}^2$$

$$EI_4 = 72.0 \text{ kN} \cdot \text{m}^2$$

The deflection at points DS2 and DS1 were calculated using a double integration bending beam calculation. Figure 7 shows the resultant combined force applied by the wing weight, testing apparatus components, and the hydraulic actuators [33]. The resultant point load was used to estimate the wing deflections, this loading however does not consider the weight distribution of the wing structure separately from the loading resulting in inaccuracy in the calculation results. The deflection of the wing at point 'x' is found using,

$$V(x) = \begin{cases} \iint \left(\frac{(x-a) \cdot F}{EI(x)} \right) d^2x, & 0 \leq x < a \\ \iint \frac{0}{EI} d^2x, & a < x \leq 2.725 \end{cases} \quad (17)$$

$$V_1(x) = \frac{F}{EI} \left(\frac{x^3}{6} - \frac{ax^2}{2} + C_1x + C_2 \right)$$

where 'x' is a function of the resultant loading force, F , at point 'a', and the change in bending stiffness, $EI(x)$. Between the root of the wing at $x = 0$ with an EI of $6.6 \cdot 10^5 \text{ Pa} \cdot \text{m}^2$ and the loading location 'a' with an EI of $6.3 \cdot 10^5 \text{ Pa} \cdot \text{m}^2$ the change in EI is less than 5%. Due to the small change bending stiffness between the root and the loading location the stiffness was considered to be constant between these two locations. The integration constants C_1 and C_2 are determined using a fixed root boundary condition.

$$V(0) = 0$$

$$\theta(0) = 0$$

The boundary conditions result in integration constants of zero. The deflection at point 'x' is found using,

$$\begin{aligned}\theta_1(x) &= \frac{d}{dx}V(x) \\ \theta_1(x) &= \frac{F}{EI} \left(\frac{x^2}{2} - ax + C_1 \right)\end{aligned}\tag{18}$$

Due to there being no change in loading between the resultant loading point and wingtip the deflection at is found as,

$$\begin{aligned}V_2(x) &= C_3x + C_4 \\ \theta_2(x) &= C_3\end{aligned}\tag{19}$$

The boundary conditions required to determined the integration constants C_3 and C_4 ensure that the deflection of the wing is continuous across the span.

$$V_1(a) = V_2(a)$$

$$\theta_1(a) = \theta_2(a)$$

The integration coefficients for the bending beam system are,

$$C_1 = 0$$

$$C_2 = 0$$

$$C_3 = \frac{F}{EI} \left(\frac{a^2}{2} - a^2 \right) - C_4$$

$$C_4 = \frac{F}{EI} \left(\frac{a^3}{6} - \frac{a^3}{2} \right)$$

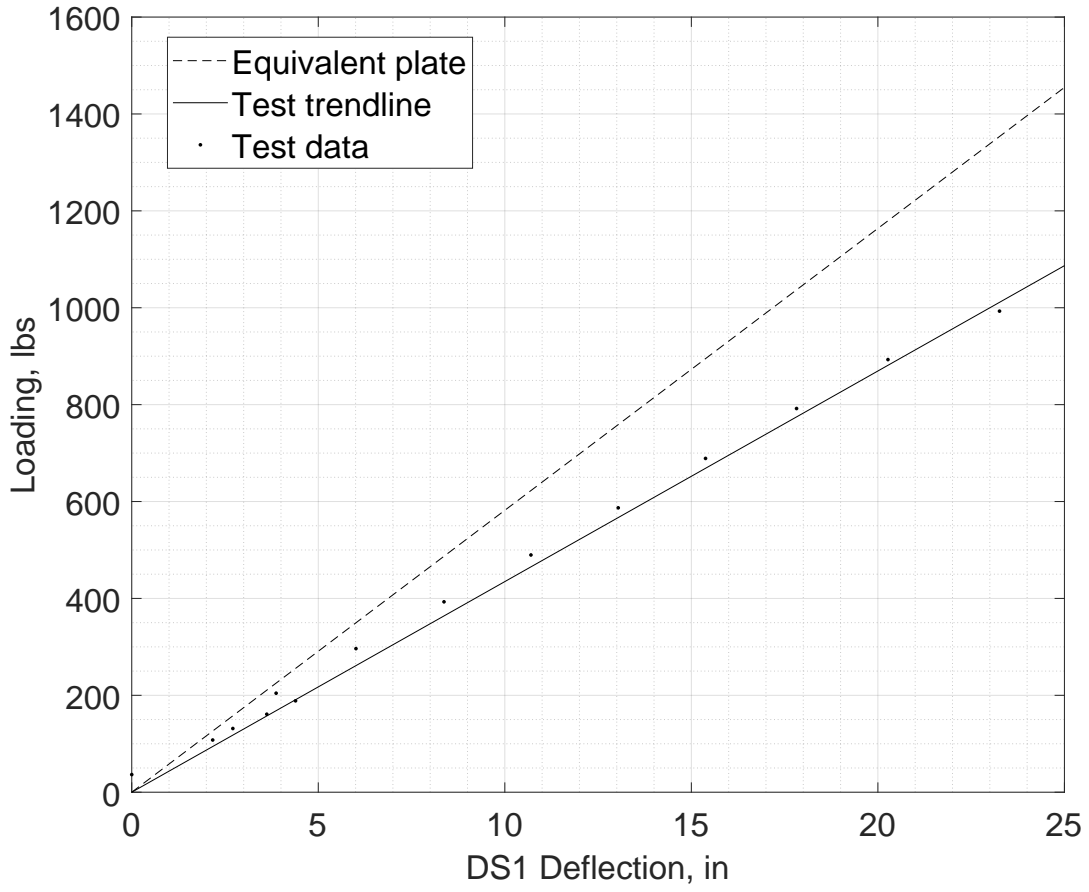


Figure 8: Comparison of equivalent plate model and experimental testing of deflections at DS1 [33].

Based on the analytical double integration cantilever method presented, using the structural parameters determined through the equivalent plate method, the wing deflections at the wingtip DS1, and at location DS2 are shown in Fig. 8 and Fig. 9, respectively. When the analytical model for the equivalent plate is compared to the experimental data a maximum of 33.0% discrepancy when evaluating the wingtip deflection and a maximum of 10.3% discrepancy is seen when evaluating the wing deflection at DS2. The differences between the equivalent plate method and test results can be attributed to the simplifications and errors as a result of the analytical model idealization. To complete a conclusive validation of the equivalent plate model an FEA analysis can be used.

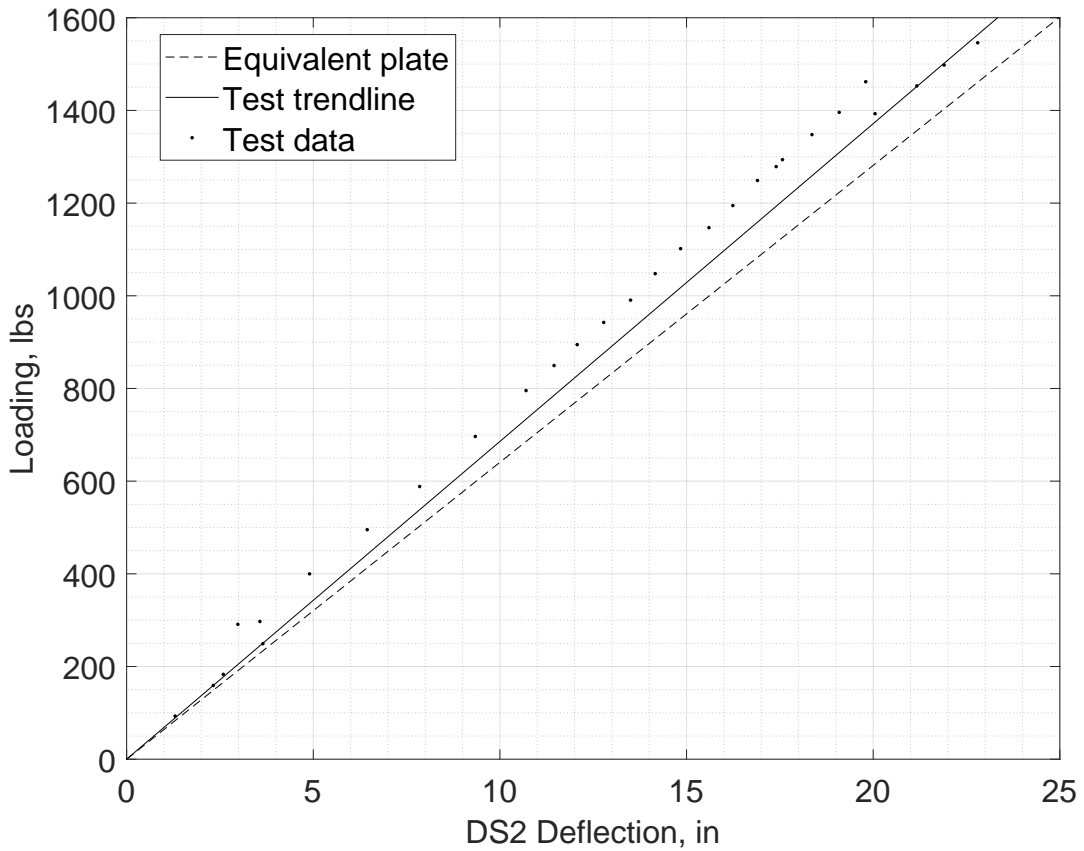


Figure 9: Comparison of equivalent plate model and experimental testing of deflections at DS2 [33].

The only data published with regards to the twisting experienced by the wing while under a purely bending load is the difference between the deflections measured at DS2 and DS3. However, location of the shear center cannot be determined with the data provided, which prevents the analytical estimation of the twist behavior under the current loading. Future explorations into the validation of the equivalent plate method in capturing the twist response is required.

4.4 Wing Section Shear Center

Structural idealization was used to locate the shear center of a wing's cross-section based on the shear properties of the composite layers and the two-dimensional geometry. The shear center location for a wing comprised of multiple materials is dependent on the material shear modulus (G), the boom area (B) of each node, and the skin thickness (t). To idealize the chosen aircraft, boom nodes are placed at the leading edge, the trailing edge, and over the spar caps on the upper and lower surfaces. Additional nodes may be added for design configurations that include spanwise stiffeners. The placement of the nodes for a NACA0010 airfoil is shown in Fig.10. The nodes are used to idealize the continuous structure as a series of boom areas with weighted structural effects.

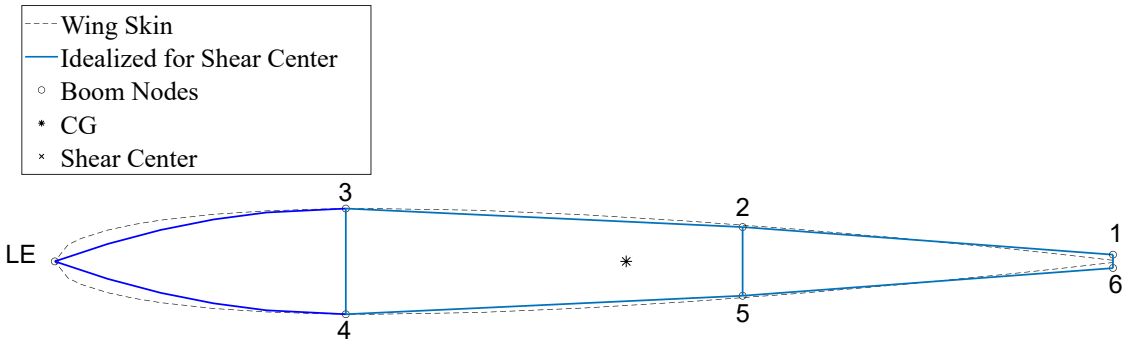


Figure 10: Structural idealization to find shear center for NACA0010.

The boom area for $node_i$ can be evaluated, based on the effects of the adjacent $nodes_j \& k$ using,

$$B = t_{skin} \cdot \left[\frac{L_{ij}}{6} \cdot \left(2 + \frac{y_j}{y_i} \right) + \frac{L_{ki}}{6} \cdot \left(2 + \frac{y_i}{y_k} \right) \right] \quad (20)$$

where, the distance between the selected node and the adjacent nodes is shown with L and the displacement of the node from the centerline is represented with y . The boom areas can be used to calculate the first area moment of inertia,

$$I_{xx} = B \cdot y^2 \quad (21)$$

and used to evaluate the shear flow through the structure. The shear flow, q , of the structure is used to evaluate the shear loading along each node, allowing for a prescribed vertical load, V_N , resulting from the expected aerodynamic loads, to be related to the deformation of the structure. To find the shear center based on the shear flow definitions the twist angle, θ_t , with respect to a vertical displacement, Z , must be equal to zero,

$$\begin{aligned} \frac{d\theta_t}{dZ} &= \frac{1}{2AG} \oint \frac{q}{t} dS \\ \frac{d\theta_t}{dZ} &= 0 \end{aligned} \quad (22)$$

where the equation is a function of the area of each cell in the structure (A), the shear modulus of the material or materials (G), and the contour of the thin wall structure (S). By defining the relationships between the shear flows at each node and creating a system of equations based on the relationships in Eq.22, the location where a change in vertical loading results in no twist deformation can be found. An example of the structural idealization used to define the location of the shear center is presented in Appendix B.

5 Design Approach

As shown in Table 1, the wing design of the selected aircraft must be completed prior to the incorporation of gust harvesting as a performance consideration. To quantify the baseline aircraft's gust energy harvesting potential, the wing geometry and initial structures, the weight breakdown, and the desired cruise conditions must be known. The process for evaluating the gust harvesting potential for a provided aircraft is shown in Fig. 11. The aerodynamic and structural parameters of the baseline aircraft are first used to estimate the ideal maximum gust energy harvesting potential, calculated using Eq. 1. The aeroelastic method presented by Melville [1] is then used to quantify the gust energy harvesting potential of the aircraft while within a prescribed gust profile. To quantify the potential gust energy harvesting improvements achievable through structural design the ideal maximum gust energy available can be compared to the gust energy harvesting potential of the baseline aircraft. If the potential improvements are determined to be significant, an optimized structure can be selected.

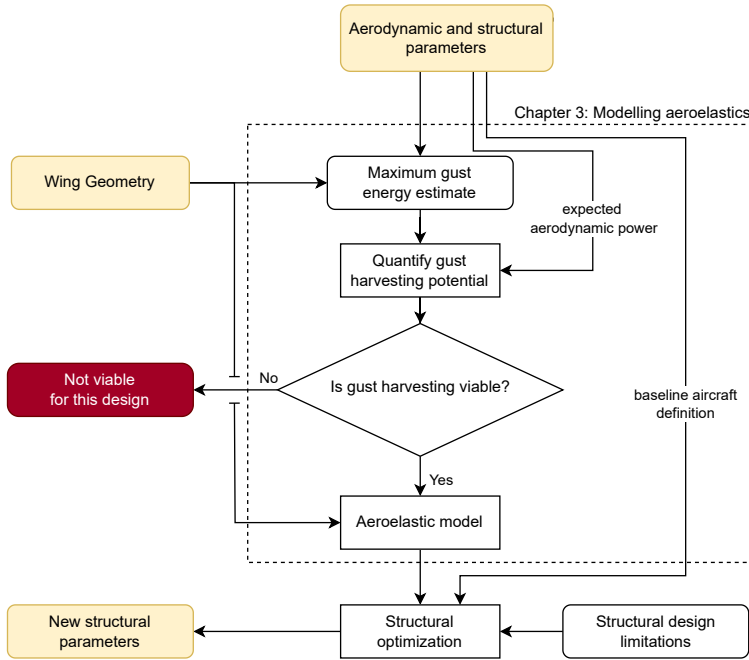


Figure 11: Baseline aircraft evaluation process.

5.1 Baseline Aircraft Evaluation

To understand if gust harvesting is viable for a chosen baseline aircraft, the aeroelastic response of the aircraft must be defined. The viability of the aircraft within a selected gust depends on both aerodynamic and structural parameters, including the expected load cases, aerodynamic performance, as well as the aircraft weight, structural stiffness parameters, and the shear center location. The aerodynamic parameters, such as span efficiency, aspect ratio, and the expected dynamic response of the aircraft within a gust are used to evaluate the maximum possible energy gains due to the gust. The theoretical maximum gust energy available is calculated to assess the achievable gains using Eq. 3.

5.2 Design Optimization

To include gust harvesting in the design stages of a viable aircraft, a genetic algorithm was used to evaluate the discrete design variables present when selecting a structure that facilitates the maximum gust energy harvesting. Figure 12 outlines the processes involved in the selection of a layup structure selected from a population of achievable composite wing structures. By developing a series of manufacturable composite wing structures, the structural parameters can be scored with respect to the agreement with the optimized structural solution from the genetic algorithm, and a proposed design was selected based on the design that minimized the weight penalties. An overview of both the genetic optimizer and the creation of the aircraft configuration population is presented in this section. An in-depth exploration of the optimization is discussed in the works of Melville [1].

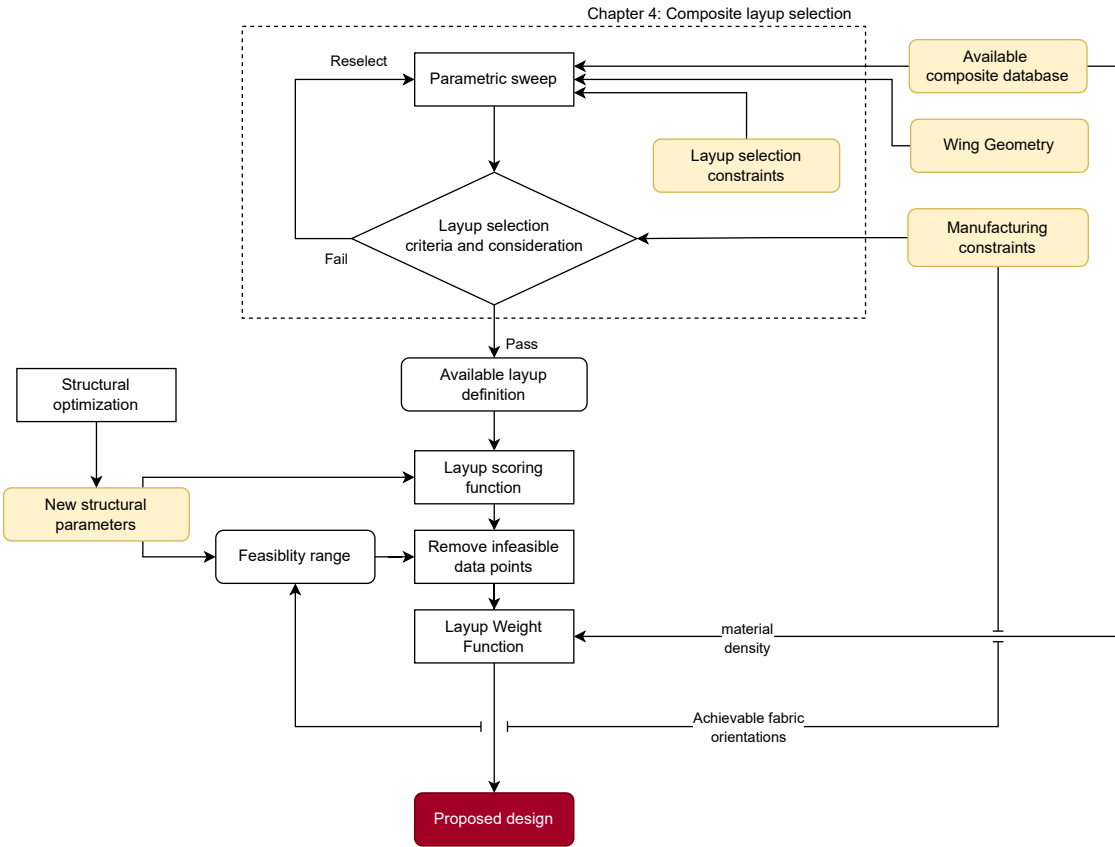


Figure 12: Optimized design selection process.

5.2.1 Structural Optimization

The optimization, implemented in the works of Melville [1, 2], explores the impact of the shear center, l_{sc} , center of gravity l_{cg} , bending stiffness, EI , and the torsional rigidity, GJ , and is utilized in this work as a method for aeroelastic tailoring. The optimization varies a range of physical constraints, defined by both mission requirements and manufacturing limitations, with the objective of maximizing the energy altitude gains when traversing a discrete gust profile.

When selecting optimizer constraints, consideration of the limiting bending and torsional stiffnesses is required to ensure that the baseline aircraft mission is achievable. These limitations include minimum and maximum EI and GJ based on layup configurations, allowable spanwise change in parameters, and the achievable center of gravity

range. The limiting stiffness values for the optimizer are selected to satisfy the minimum bending and torsional response required for the operation of the aircraft, and constrained to fall within a range of acceptable layup configurations. A parametric sweep is completed to identify the range of acceptable layup configurations by evaluating all possible configurations based on the acceptable ply orientations, available fabrics, and the maximum number of layers. To avoid discontinuities and stress concentrations limits are enforced across the span to prevent large changes in stiffness between each element. By constraining the optimizer a structure is selected from within the prescribed layup configuration range.

The center of gravity for a wing section and the relationship to the shear center are constrained by the acceptable weight distributions and the acceptable changes in wing geometry. The shear center location is dependent on both the geometry of the wing section and the material properties. By constraining the spar locations and the outer wing geometry, only alterations in the skin thickness through layup selection and the accompanying shear modulus changes will change the shear center location. The calculation of the shear center location as a result of a specific wing section configuration is outlined in Appendix C.

5.2.2 Layup Selection

As seen in Fig.12 an achievable layup population is generated based on user-specified constraints. The structural performance of each configuration is then ranked in comparison to the optimized stiffness parameters, and the shear center locations. For this evaluation, the center of gravity is assumed to be altered through ballast or weight balancing rather than included as a constraint in the structural design, as a change in layup only has minor effects on the center of gravity due to the constant geometry.

A range of composite fabric layers are considered in the design space by including null layers as a material selection. The composite fabric parameter includes the null layer and all the available composite fabrics, either from an online database or what is currently

accessible, allowing the population to be limited to desirable materials. Depending on the layup method and the composite weave styles available, some ply orientations are not achievable due to manufacturing limitations. By defining achievable ply orientations for the design space, the number of cases is reduced, and further tuning of the geometry can be completed if higher accuracy ply placement techniques are available. In the case where a plain woven fabric is used, ply orientations of [-45/45], [0/90], and [-30/60] allow for the effects of high bending stiffness, shear stiffness, or bending-twist coupling to be captured in the design depending on the orientation selected. The sandwich core thickness is selected based on the desired increase in moment of inertia for the wing skin, both to prevent buckling and increase ground handling reliability. By defining every layup configuration within the scope of the listed constraints, limits on the achievable stiffness values and shear center locations are defined for use with the optimization results. The upper and lower bounds for the optimizer is then dependent on the available composite material and realistic manufacturing constraints.

After the optimized structural parameters are selected, and the layup configurations are populated, each layup is scored based on the agreement of the specific configuration's stiffness values and shear centers determined through the use of the equivalent classical plate method. The scoring function is,

$$F = W_{EI} \cdot \frac{EI_{des} - EI_x}{EI_{des}} + W_{GJ} \cdot \frac{GJ_{des} - GJ_x}{GJ_{des}} + W_{sc} \cdot \frac{e_{des} - e_x}{e_{des}} \quad (23)$$

where the desired structural parameters are denoted with the subscript *des* and the available layup configurations, denoted with the subscript *x*. Each parameter is assigned a weight, denoted as *W*, to emphasize the importance of different parameters. A smaller weight, relative to the others, indicates less importance placed on that variable. For example, the location of the shear center can be shifted through small changes in the placement of the stiffeners; the bending and torsional stiffness almost entirely depend on the wing skin and spar cap layup selection. The layups with the lowest score represent

the configurations that conform more closely to the desired structural parameters and are selected as design candidates. However, the layup with the lowest score may not be the most realistic or optimal choice, depending on other selection considerations. Based on the discussed scoring parameter and the manufacturing irregularity study, shown in Fig.1, a feasible range of layups is selected. A feasible layup configuration features structural parameters within a range of bending and torsional stiffness values centered around the target optimized parameters. Setting a feasibility range increases the number of acceptable layup configurations, allowing for the selection of a layup that, when considering the limitations of the manufacturing accuracy, still conforms to the desired structural performance. Within the range of feasible layup configurations, the available layups are ranked based on the physical weight penalty of each design and selected accordingly. By allowing for a broader range of acceptable layups to be considered, a lighter-weight structure may be chosen. The chosen core thickness is constant across the span to prevent kinks in the composite laminate and stress concentrations.

The design approach presented in this chapter outlined the considerations required to include gust harvesting in the preliminary wing design stages. Considering the available materials and the baseline aircraft, a metric to quantify the possible performance benefits and the available layup configurations was outlined. Through the application of a genetic algorithm, a set of aeroelastically tailored structural parameters can be selected to increase the gust harvesting efficiency of the aircraft. The designs that satisfy the desired structural constraints can be selected based on manufacturing ease and the overall weight of the new design. The design approach presented is applied in Chapter 5 to evaluate a known aircraft and propose a new layup configuration.

6 Results and Case Study

The design approach proposed was used to evaluate the design of an uncrewed aerial system (UAS), known as *SW117*, operated and manufactured by Superwake, a research and development company. The aircraft used for the following case study is shown in Fig.13 and the aircraft parameters are presented in Table 2.

Wing span (m)	5.24
Mass (kg)	25
Cruise speed (m/s)	18
Wing loading (kg/m^2)	11
Aspect ratio	13.6

Table 2: SW117 aircraft parameters.

The operation-focused aircraft was developed with the intention of completing long-term surveillance operations such as wildlife monitoring. The design of the aircraft resembles a sailplane with a large aspect ratio and low wing-loading. The SW117 aircraft was selected for redesign to increase the achievable flight endurance through passive gust energy harvesting through aeroelastic tailoring. The design approach is shown in Fig.11 and 12, and outlined in Chapter 4 was used to propose a new composite structure.



Figure 13: Solar powered UAS, “*SW117*”. [34]

The SW117 aircraft is a good case study to showcase the benefits of gust harvesting due to the wide range of acceptable bending and torsional stiffness values for the proposed design. The current baseline aircraft has a composite wing structure supported by two spars and a sandwich composite skin comprised of a core material between two layers of structural fabrics oriented at [-45/45] that are uniform across the wingspan.

Before the performance of the selected baseline aircraft can be evaluated, the stiffness values and shear center had yet to be determined. Estimates of the input parameters were found using the equivalent plate method and structural idealization outlined in Chapter 4.

The cross-section of the wing, shown in Fig.14, is equivalent to the laminate plate shown in Fig.15. Figure 14 includes the idealized structure used to find the shear center location. By completing the equivalent plate analysis the bending and torsional rigidity of the baseline wing were found to be:

$$EI = 9.66 \text{ kN} \cdot \text{m}^2$$

$$GJ = 6.35 \text{ kN} \cdot \text{m}^2$$

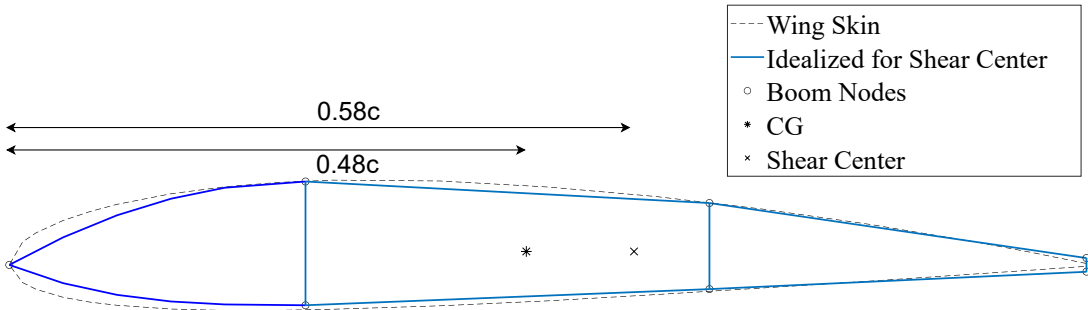


Figure 14: Baseline aircraft cross-section and idealized structure for shear center evaluation.

(Scaled by undisclosed factor to protect proprietary information)

The baseline aircraft has a constant cross-section and a rectangular planform, thus the stiffness values and shear center location are also constant across the wingspan. The bending stiffness of the wing is primary a result of the spar caps. These are comprised

of multiple layers of unidirectional tape. For any new design, the spar cap configuration was held constant to ensure that the required bending stiffness was achieved; at the same time, the skin layup was altered to tailor the aircraft's structural response.

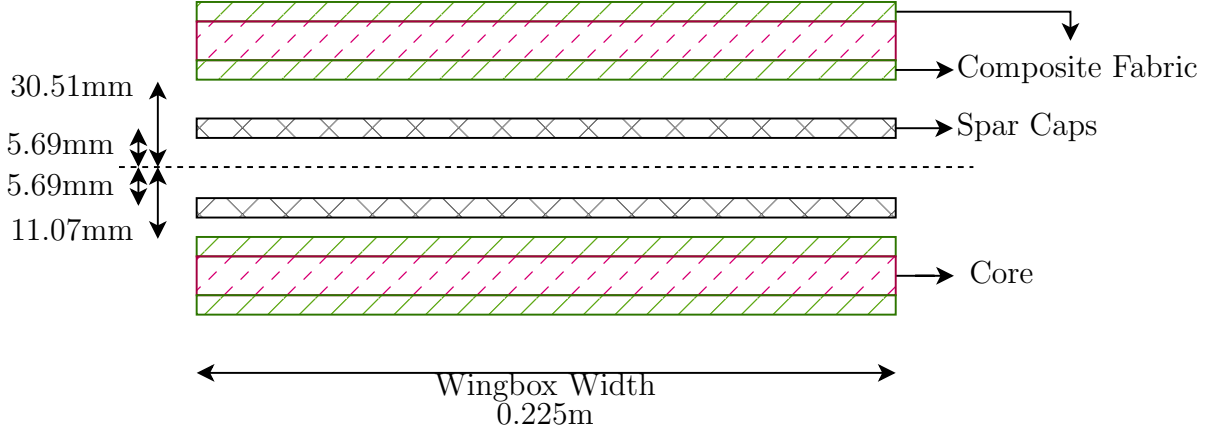


Figure 15: Equivalent plate reduction of baseline wing cross-section along the X-Z plane.
(not to scale)

The baseline aircraft design, shown in Fig.14, was equated to a set of four plates as shown in Fig. 15. For the equivalent plate model the spar caps begin at a different location then the wing skin to maintain the moment of inertia between the initial thin structure that is then stretched to be the same width as the equivalent plate. The thickness and location of each layer, labeled from the upper surface down, were altered to ensure the moment of inertia of each material is conserved. The sandwich structure is summarized in Table 3.

	Thickness (mm)	Ply Orientation (deg)
Layer 1	0.217	Fiberglass [-45/45]
Layer 2	2.718	Core
Layer 3	0.203	Carbon Fiber [-45/45]
Layer 4	0.009	Unidirectional Carbon Fiber [0]

Table 3: Baseline aircraft sandwich structure.

The SW117 aircraft is an interesting design case when considering gust energy harvesting, thank to the large structural design space, relaxed structural constraints, and the low operating speeds and wing loading. The current structural parameters are estimated through the application of structural idealization and classical laminate plate theory to provide estimations of the expected performance.

6.1 Baseline Aircraft Performance

The baseline configuration's performance was evaluated across a range of discrete sinusoidal gusts to quantify the maximum potential gains. Figure 16 compares the performance of the baseline aircraft, defined using Melville's [1] aeroelastic model, against the idealized energy altitude gains determined through Eq. 1. In the same figure, the performance of the baseline aircraft with a rigid structure is presented. The differences in performance between the current flexible structure and the rigid aircraft are negligible. This negligible difference is not unexpected, as the current wing, was designed to minimize deflections to protect the solar array. The difference between the energy altitude gains of the baseline aircraft and the theoretical maximum gains defines the maximum energy available for the current aircraft through aeroelastic tailoring.

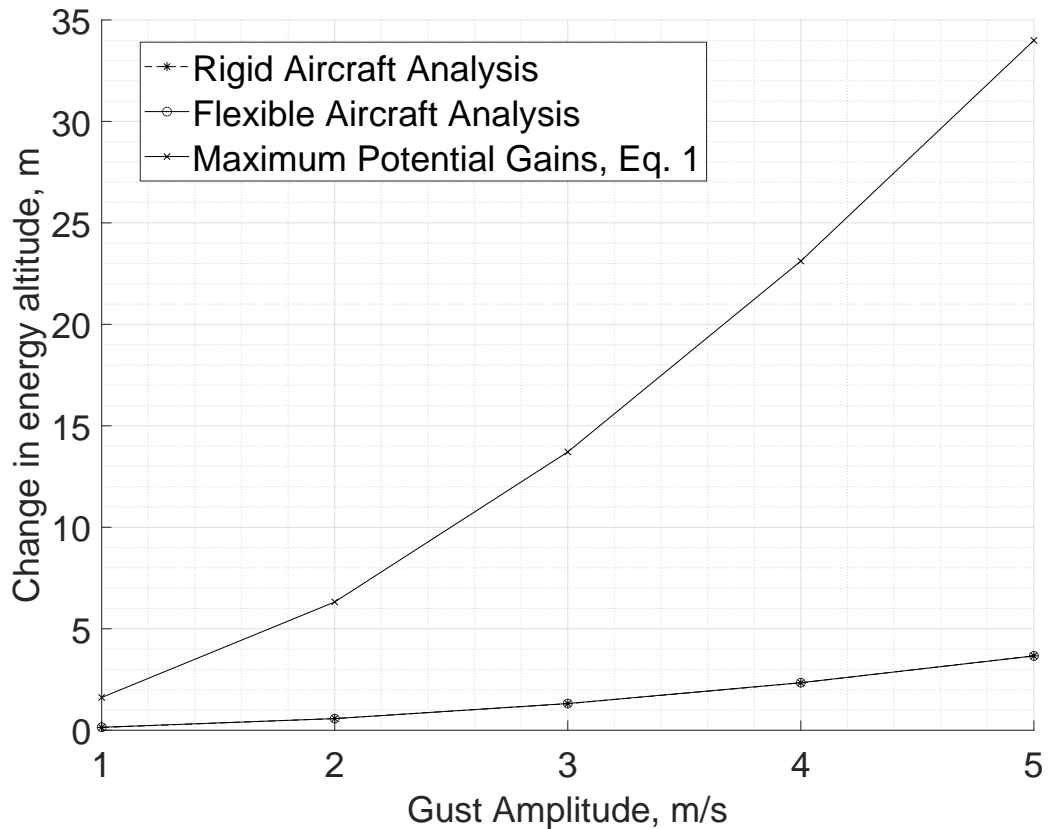


Figure 16: Energy altitude gains of *SW117* aircraft passing through a sinusoidal gust.

The gust response for the SW117 aircraft within a gust with a length of 30 m and a maximum amplitude of 5 m/s was evaluated in this case study. Gust amplitude of 5 m/s result in the angles of attack that exceed post-stall angles of 22° . The aerodynamic model is unable to adequately capture stall and beyond.

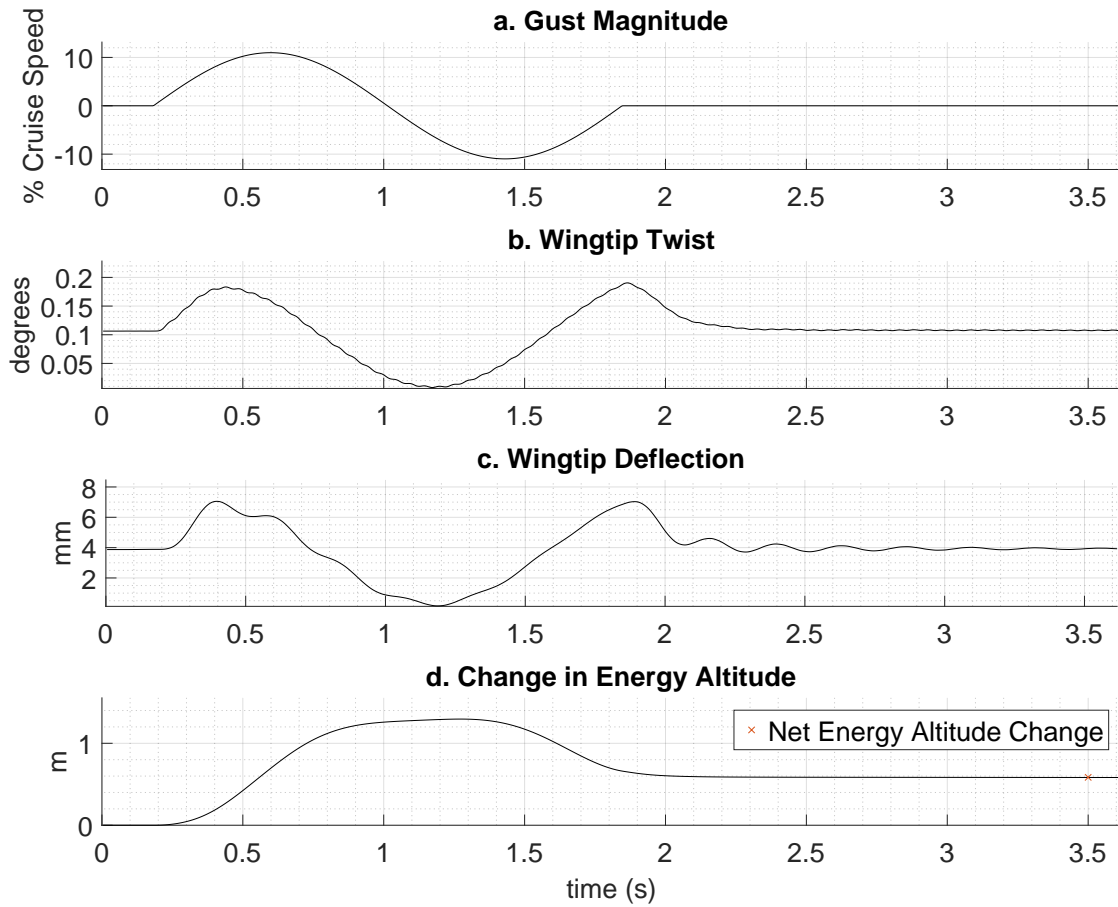


Figure 17: Baseline aircraft performance within a gust: (a) gust profile; (b) wingtip twist; (c) wingtip deflection; and (d) energy altitude gains.

Figure 17 shows the structural response and the resulting change in the energy altitude of the baseline aircraft as it traverses through a discrete sinusoidal gust with an amplitude of 2 m/s. The aircraft wingtip twist and bending deflections are shown in Fig.17b and c. The change in energy altitude is shown in Fig.17d. After exiting the gust and the aircraft returns to the original steady-state and a net energy altitude gain can be seen. The net change in energy altitude represents the change in the energy state of the aircraft due to the gust that has a net-zero effect on the airmass.

6.2 Structural Optimization

To optimize the structural parameters, a genetic algorithm was employed to evaluate discrete aircraft configurations within a specified range [1, 35]. The optimizer evaluated the effects of varying bending stiffness, torsional rigidity, and the shear center at each spanwise element. Figure 18 shows a top-down view of the wing halfspan with 16 spanwise elements. The optimizer was limited to change the stiffness and shear center location no more than 5% between adjacent elements. This limitation helps prevent structural discontinuities that could lead to stress concentrations or unrealistic layup configurations.

Additional constraints were imposed on the upper and lower bounds of bending and torsional stiffness, based on the minimum and maximum achievable values within the design space. These bounds reflect the feasible layup configurations determined by the available materials and acceptable design parameters. By enforcing constraints on both the relative changes and the allowable ranges of the parameters, the resulting design is ensured to remain within the feasible design space.

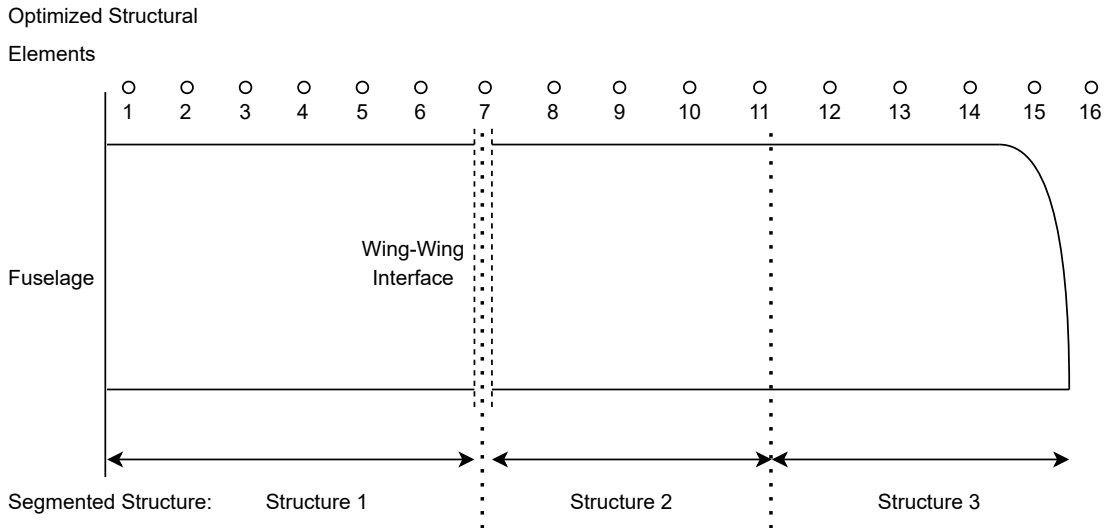


Figure 18: Wing panel structural configurations of wing halfspan.
(*Not to scale*)

Through the use of the outlined structural optimization and the works of Melville [1–3], a new series of structural parameters was selected. The optimized structural parameters that were varied during the optimization problem are presented in the first column of Table D.1 in Appendix D. These parameters resulted in an aircraft with a larger gust harvesting potential when compared to the baseline aircraft. The aeroelastic tailoring optimizer determined structural parameters for each spanwise structural element, as shown in Fig. 18.

Although the optimized values result in a configuration that has a higher gust energy harvesting performance, the optimized configuration is unrealistic to manufacture due to the structural parameters changing at each element. To reduce the number of composite layups required to achieve the desired performance the wing is broken into three segments, two in the outboard and one for the inboard as shown in Fig. 18. The structural parameters for each segment of the wing panels are an average values of the optimized spanwise structural element. The averaged spanwise structural elements are shown in the last column of Table D.1 in Appendix D. Segmenting the wing panels simplifies manufacturing at the cost of reducing the energy harvesting capability of the aircraft. Nevertheless, the performance of each configuration shows that minor changes to the structure resulted in small changes in gust harvesting potential under a range of vertical sinusoidal gusts of 1 m/s to 5 m/s. The changes in energy altitude that are shown in Table 4, show that the change in performance due to the segmentation is not significant. The numerical representation of the segmented configuration was used to select a wing skin composite layup that achieves the desired parameters.

Table 4: Performance of optimized and segmented configurations.

Gust Magnitude (m/s)	Optimized Δz_e (m)	Segmented Δz_e (m)
1.0	0.157	0.155
2.0	0.629	0.618
3.0	1.42	1.39
4.0	2.52	2.48
5.0	3.94	3.87

6.3 Layup Selection

To define the layup configuration design space for the case study the configurations were constrained based on the available materials, the acceptable ply orientations, and the number of layers allowed in the upper and lower wing surfaces. Figure 19 shows the design space for the current case study, representing each available layup configuration as a point. The three wing segment points represent the three wing segments that were selected through the structural optimization. Each desired point has a feasibility range that represents the range of layup configurations that closely satisfy the desired structural parameters. The selection of a point within the feasibility ranges results in a structure that achieves the desired bending and torsional stiffness.

For this case study a database of materials was selected based on materials that are readily available. One fiberglass and one carbon fiber weave were selected along with one unidirectional carbon fiber used for the spar caps. Ply orientations of [-45/45], [-30/60], [30/-60], and [0/90] were chosen to be included in the design space. The selected ply orientations capture maximum torsional rigidity, maximum wash-in effects, maximum wash-out effects, and maximum bending stiffness respectively. The number of layers for the upper and lower surfaces was selected to range between 1-5 layers, with the a core material of either 1 or 2 mm in thickness. A maximum of 5 layers captures the range of bending and torsional rigidities required to select the desired layup configurations. The limits imposed constrain the parametric sweep that utilizes the equivalent plate model and classic laminate plate theory to determine the bending and torsional stiffnesses.

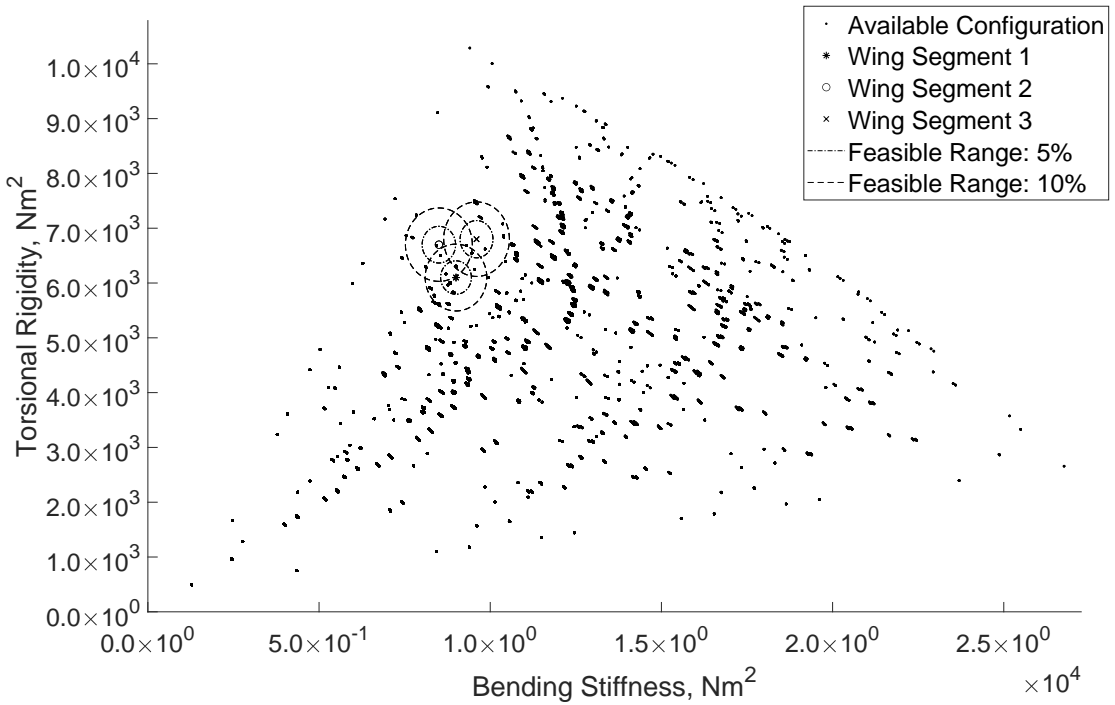


Figure 19: Achievable wing structural properties based on available composite materials and manufacturing constraints.

The selection of an appropriate composite structure must consider the stiffness parameters as well as other design considerations such as the shear center, the weight of the selected layup, and the continuity of the layup between each panel segment. To include these design considerations in the selection process the feasibility range is used to select a range of configurations that are acceptable, this process is repeated for all three segments, as shown with the configuration points in Fig. 19. To reduce the weight and the manufacturing complexity the minimum core thickness is selected that achieves the desired stiffness. For this case study a core thickness of 1 mm is shown to be acceptable to achieve the desired structural parameters.

By scoring each composite layup configuration using Eq. 23, a composite layup was selected for each of the three segmented wing panels. The layups selected for each segment are shown in Table 5. While the layups selected achieve the desired structural parameters for each of the three segments, Fig. 19 shows there is a number of composite layup configurations in-between the three segments. The first layer in the upper surface is

constrained to be [-45/45] fiberglass weave in order to incorporate the solar array, which must be isolated electrically.

Table 5: Segmented composite layup at 3 spanwise locations.

	Segment 1	Segment 2	Segment 3
Upper Surface	Fiberglass Weave, [-45/45]	Fiberglass Weave, [-45/45]	Fiberglass Weave, [-45/45]
	Core, 1mm	Core, 1mm	Core, 1mm
	Carbon Weave, [-30/60]	Carbon Weave, [-45/45]	Carbon Weave, [-60/30]
Lower Surface	Carbon Weave, [-60/30]	Carbon Weave, [-60/30]	Carbon Weave, [-30/60]
	Core, 1mm	Core, 1mm	Core, 1mm
	Carbon Weave, [-45/45]	Carbon Weave, [-30/60]	Carbon Weave, [-45/45]

In order to simplify manufacturing even further, a single layup schedule was explored for the entire wingspan. The subsequently selected single layup that satisfies the three desired segments is shown in Table 6. The gust energy harvesting performance of the single composite layup configuration of Table 6, is compared to the gust energy harvesting potential of the segmented configuration of Table 5 in Section 6.4.

Table 6: Single composite layup selection.

Upper Surface	Fiberglass Weave, [-45/45] Core, 1mm Carbon Fiber Weave, [-60/30]
Lower Surface	Carbon Weave, [-30/60] Core, 1mm Carbon Weave, [-45/45]

The bending and torsional stiffness distribution for the four aircraft wing configurations that are considered are shown in Fig. 20 and are compared to the baseline aircraft's constant structural properties. The optimized aircraft configuration compiled in Appendix D varies across each spanwise structural element and is related to the 3-segment designs through the averaging of the spanwise elements between 0 to 6, 7 to 11, and 12 to 16. Spanwise elements 0 to 6 represent the inboard, as shown in Fig. 18, while outboard is represented with elements 7 to 16. The gust energy harvesting potential of each wing configuration is discussed in the following section.

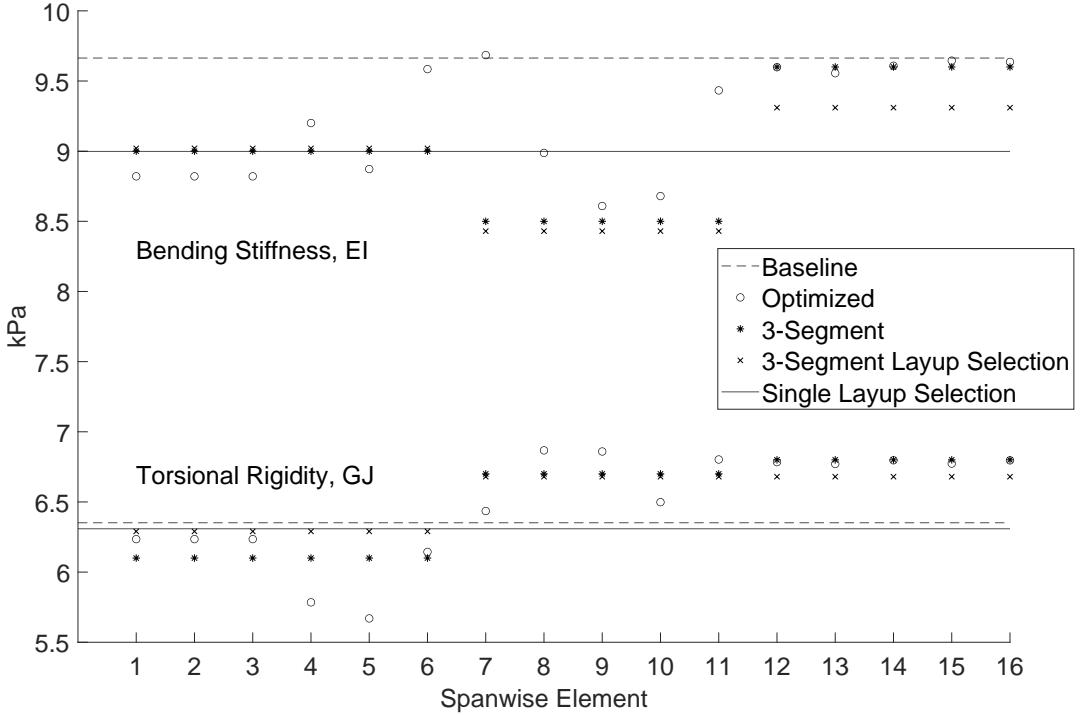


Figure 20: Bending and torsional rigidity structural element distribution for given half-span configuration.

The bending stiffness is reduced by comparison to the baseline design for the four selected wing configurations shown in Fig. 20 while the torsional rigidity on average is reduced. The work of Melville [1] found that increasing the bending stiffness decreasing the torsional rigidity could result in an increased gust energy harvesting potential for the chosen aircraft. The bending stiffness in the selected cases is shown to be lower, disagreeing with the results of Melville [1]. However, due to the low aerodynamic loads, and the low resulting bending, the 6% decrease in bending stiffness seen results in only minor changes to the bending behavior of the wing. The structural response of the proposed wings and the accompanying gust energy harvesting performances are presented in the following section.

The torsional stiffness is shown to be reduced for the inboard section and is shown to be stiffer in for the two outboard sections for the 3-segment configuration. With the moment experienced by the wing being greatest at the root, a low bending stiffness at

the root will result in the largest effect at the wingtip. The gust energy harvesting for each of the four wing configurations is presented in the following section.

6.4 Proposed Aircraft Configuration Performance

In Table 7 the gust energy harvesting performance, represented as a change in energy altitude, for the baseline aircraft is compared to the performance of the segmented design, the composite structure that satisfy those segments, and a mid-way point that satisfies all three wing segments. Negligible changes in energy altitude gains where seen as a result of the change in structural parameters between the optimized segmented wing configuration and the achievable layup configuration for each segment. All three redesigned wing configurations performed better then the baseline aircraft with a maximum predicted energy altitude gain of 6.1% for the 3-segment wing configuration. The single continuous composite wing configuration gained less then half the gust energy harvesting performance improvements by comparison to the 3-segmented configuration.

Table 7: Performance of baseline and final configurations.

Gust Magnitude (m/s)	Baseline $\Delta z_{e,b}(m)$	3-Segment		3-Segment Composite Layup Selection		Single Composite Layup Selection	
		$\Delta z_e(m)$	$\Delta z_e/\Delta z_{e,b}$	$\Delta z_e(m)$	$\Delta z_e/\Delta z_{e,b}$	$\Delta z_e(m)$	$\Delta z_e/\Delta z_{e,b}$
1.0	0.146	0.155	1.061	0.155	1.061	0.148	1.014
2.0	0.583	0.618	1.060	0.618	1.060	0.591	1.014
3.0	1.31	1.39	1.061	1.39	1.061	1.33	1.015
4.0	2.34	2.48	1.060	2.48	1.060	2.37	1.012
5.0	3.65	3.87	1.060	3.87	1.060	3.70	1.014

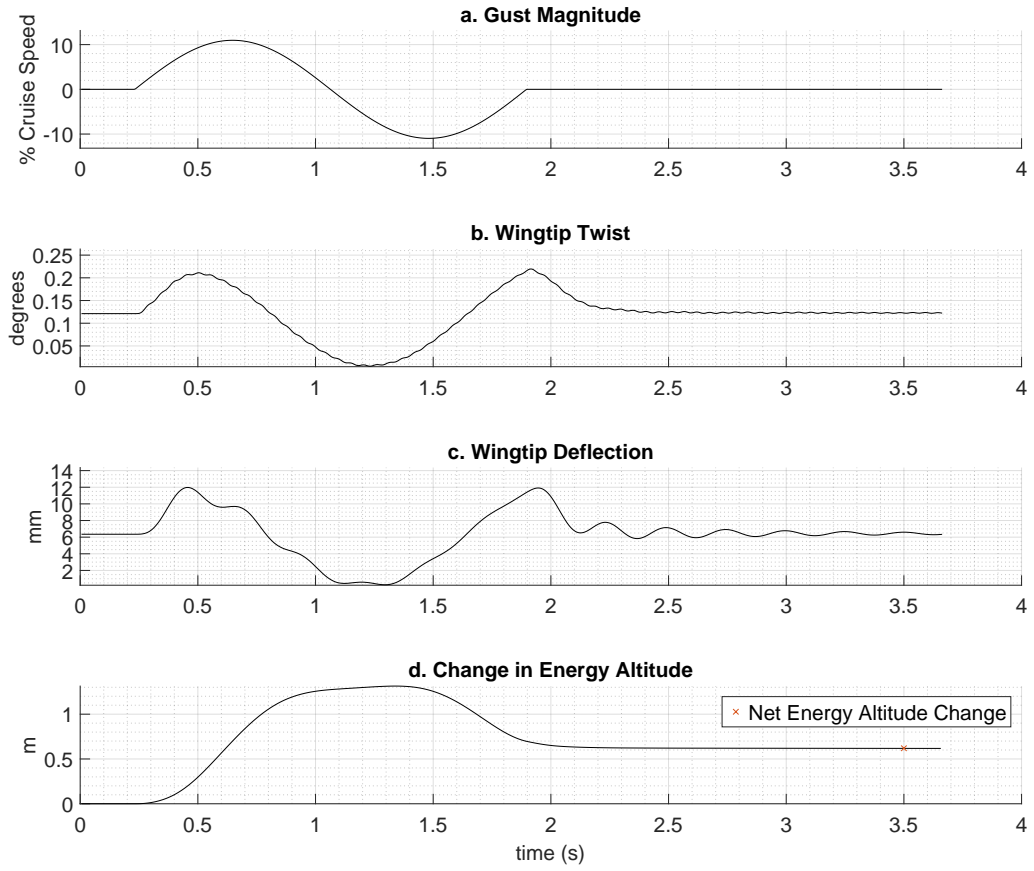


Figure 21: 3-Segment aircraft configuration performance within a gust: (a) gust profile; (b) wingtip twist; (c) wingtip deflection; and (d) energy altitude gains.

The change in energy altitude while pass through a 2 m/s sinusoidal gust is shown in Fig.21 for the segmented wing configuration. By comparison to the structural response of the baseline configuration, shown in Fig.17, the tip twist is seen to be 15.7% larger. The change in energy altitude, shown in Fig. 21d has two section of interest, the first section around 0.5 seconds shows a sharp increase in energy altitude while the aircraft is within the upward section of the sinusoidal gust. The second section of interest begins around 1.5 second when the aircraft experiences the downward portion of the gust and losses energy altitude. The effect that the negative affect that the gust has on the energy state of the aircraft is smaller then the benefits of the upward portion. The change experienced within the downward portion is smaller due to the increase in drag due to the tilting lift vector being smaller within a downward gust when compared to

the magnitude of the drag reduction seen while within a vertical gust. The selection of a segmented wing configuration that features lower torsional rigidity resulted in an increase in the gust energy harvesting performance for the vehicle when compared to the baseline configuration.

The change in the structural response for the finalized segmented configuration, by comparison to the baseline aircraft, agrees with the expected conclusions of Melville [1]. Melville [1] showed that an increase in the twist experienced across the wing and a reduction in deflection would result in an aircraft with increase gust energy harvesting potential. The segmented design resulted in an aircraft that experienced 15.7% more twist and greater deflection. However, the deflection change is less than 5%, resulting in the effects on the aerodynamic performance of the aircraft to be minor when compared to the more significant changes in twist.

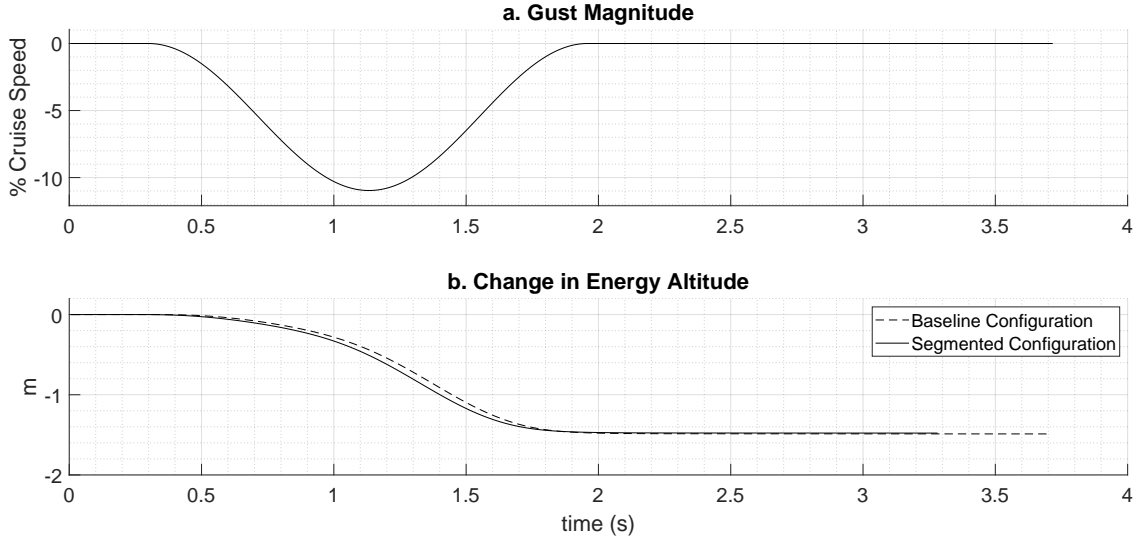


Figure 22: Change in energy altitude for baseline and final segmented aircrafts within a discrete downward gust.

Figure 21 shows how the energy state of the aircraft changes throughout the flight while within a discrete sinusoidal gust, which allows for an understanding of the overall change performance of the aircraft by comparison to the baseline. To show that the aircraft performs better than the baseline aircraft the change in energy altitude due to a

downward gust is shown in Fig. 22. The reduction in energy altitude losses within the downward gust in comparison to the baseline aircraft, is around 0.67% for the segmented configuration.

By comparison to the 6.1% change seen when traversing the gust with a net-zero effect on the airmass the change in performance while within a purely downward gust is much smaller when compared to the baseline. The change in performance being small is to be expected due to the change in drag, as a result of the tilting lift vector, being smaller when compared to the drag changes experienced while within an upward gust.

Due to the all three configurations requiring the same number of layers of carbon fiber and fiberglass weave, and only varying the ply orientation and placement, the resultant weight for each configuration is essentially the same. An expansion of the composite material database, currently defined based on the available materials, will result in larger number of viable structural configurations that could have been ranked based on the final structural weight.

Through the selection of a composite wing structure the performance of the baseline aircraft was shown to increase by upwards of 6.1% while traversing a gust. While traversing a 2 m/s sinusoidal gust the net energy altitude gains were shown to be 0.618m. This net change in energy altitude equates to a total power required reduction, calculated using Eq. 6, of 101.0 Watts for the case study aircraft that weights 25kg and traversed a 1.5 second gust. The power savings were shown to be significant while traversing a sinusoidal gust for the 3-segmented design when compared to the 95.3 Watts for the baseline design. Purely through structural design the power required for the case study aircraft was shown to be reduced by 5.7 Watts.

7 Future Work and Development

By considering the available design space for the SW117 aircraft, composite skin layups were explored for their gust energy harvesting potential through the change in the structural response. Future work on this study will include the structural testing of the current airframe, the manufacturing of a new set of wings, and flight testing to quantify the achievable gains through gust harvesting.

The goal of this work is to comprehensively describe and quantify the complete method for taking a proposed aircraft and determining the real-world energy savings through gust harvesting. The discussion presented in this thesis outlines the simulated gust harvesting potential of the proposed design and the numerical representation of the baseline aircraft; however, future explorations are required to evaluate the experimental structural performance of the baseline aircraft, and flight testing is required to evaluate the experimental gust energy harvesting of both the baseline and the final segmented designs.

7.1 Structural Testing

Methods similar to the whiffle tree loading and support structure implemented by Sullivan et al. [33] can be used to evaluate the bending and twist response of the baseline aircraft. A whiffletree testing apparatus, as shown in Fig.23, allows for the structural testing of a wing through the measurement of the spanwise and chordwise deflections. Cradles, clamped to the surface of the wing serve as support, location to measure deflection, and location to apply the test loads. The loading can be accomplished through hydraulic means, similar to the method used by Sullivan et al. [33], or through electromechanical loading actuators. However, a simplified and cost-effective method, such as hanging weights, allows for the static structural testing of the bound airframe. As seen in Fig.23, the proposed configuration loads the airframe downward for simplicity. This loading requires the weight of the wings and the cradles to be considered along with the

manufacturing supporting elements to be included for the standby scenario so as not to excessively load or permanently deform the structure.

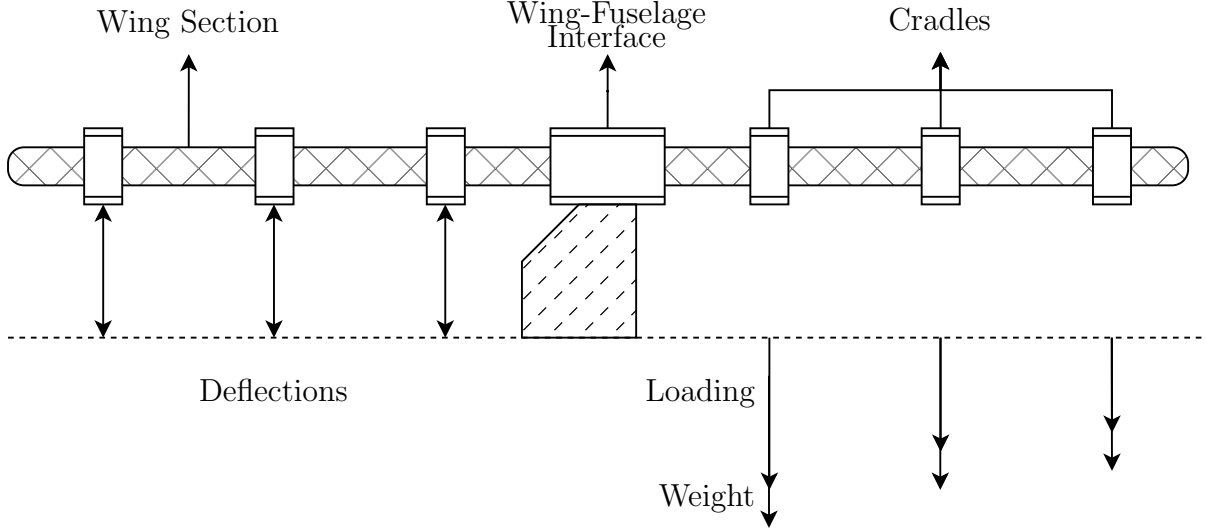


Figure 23: Proposed whiffletree configuration for structural testing [33].

For this testing, it is essential to consider that when comparing the results to the simulated static deflections, there are real-world considerations not included. Most important for the SW117 aircraft is the wing-wing interfaces that feature a connecting structure that will experience deflections differently than a continuous structure. Other considerations include considering the clamping locations, the affixing of the wing-fuselage interface to the test mount, the load distribution, and the required number of cradles to achieve this. The proposed development of a whiffletree apparatus allows for scalable and repeatable testing of various airframes to build an understanding of the baseline airframe's static structural response.

7.2 Flight Testing

A challenge to overcome when quantifying the gust energy harvesting potentials for two different wing configurations, is the irregularity and uncertainty of the gust conditions experienced during flight. In an ideal world, two identical flights would be completed for both the baseline aircraft and the new proposed design, allowing for a direct performance

comparison. Apart from completing hundreds of flights and comparing gust data and overall performance data for the two aircraft, which is both time-consuming and expensive, flight testing methods in-flight that compare the performance of the two wings may be possible.

Studies have been completed on asymmetric aircraft in the past by research institutes such as NASA [36, 37]; these asymmetric wings unevenly apply moments to the aircraft that are counteracted by trimming the aileron and rudder. The moments experienced by these aircraft, such as the AD-1 with a pivoting wing [38], provide information to the pilot through the required response. Following the same logic, manufacturing two wing sections where the wing to the right of the fuselage follows the baseline design and the wing to the left follows the new proposed design would allow for a comparison of the performance of each wing through the required control surface inputs. By manufacturing one aircraft that features both wing designs, the same gust conditions can be achieved during a single flight.

The proposed flight testing method introduces many unknown factors but allows for a more direct comparison between the gust harvesting potential of the two structural configurations. For starters, a symmetric weight distribution of the two wings is needed in order to ensure the only difference between the two wings is due to the structure. An in-depth understanding and measurement of the movement of the atmosphere around the aircraft is required to ensure the gusts experienced are adequately captured and represented in the data. Other considerations are necessary to properly measure the loading experienced. While being able to flight test both the baseline and the proposed design within the same gust is interesting and warrants further study, many design and testing constraints will require careful exploration and isolation to ensure they do not affect the results.

8 Conclusion

What performance gains are possible through gust energy harvesting for a small, high-endurance, UAS using aeroelastic tailoring methods? Through the application of aeroelastic tailoring, the gust energy harvesting performance of the SW117 UAS was shown to increase by 6.1% while traversing a sinusoidal gust. By simulating the gust energy harvested within a sinusoidal gust for the final design and comparing it to the baseline aircraft, the proposed 3-segment design was shown to be the configuration that gains the most energy within upwards gusts and lose the least energy while within downward gusts. Thus, through aeroelastic tailoring the performance of a UAS can be improved, especially for a turbulent atmosphere.

What structural design parameters are most relevant when considering gust-energy harvesting? Through the application of a genetic algorithm, an optimized wing configuration was selected that features a similar structural response in bending and increased twist when compared to the baseline aircraft. The torsional rigidity of the wing structure was found to have the most significant effect on the gust energy harvesting performance of the aircraft. However, the use of composite weaves results in torsion and bending stiffnesses being inversely related, resulting in an increase in torsional stiffness resulting in a decrease in bending stiffness when maintaining the number of plies.

What fidelity of modeling is required to determine the influence of a composite layup schedule on the relevant structural parameters? This thesis outlined that applying a low-fidelity equivalent plate model that idealizes a thin wing section as a single equivalent plate can be used to estimate the structural parameters for a rectangular or tapered wing. The modeling of a composite wing as a laminate plate allows for quick evaluations to be completed on thousands of available layup configurations. By evaluating many composite wing configurations, a selection process was used to score and determine a structure with the highest gust energy harvesting potential. Using an equivalent plate model to idealize a wing structure allows for a parametric sweep of many

composite wing structure's to be evaluated quickly using classical laminate plate theory. The use of the equivalent plate model greatly reduced the computational costs associated with the structural configuration selection process in comparison to other computationally intensive models such as FEA.

What are the limitations of gust energy harvesting and how can an appropriate structural design space be selected? While gust energy harvesting serves as a passive method to increase the performance of a given aircraft, limitations on the structural design space result in limited gust energy harvesting gains. A flexible wing structure is desired to improve the energy gained while within a gust; however, structural constraints on the aircraft limit the feasible designs. The design limitations as a result of manufacturing constraints can be quantified through the application of a parametric sweep that evaluates and scores a range of achievable composite wing structures. To quantify the composite wing design limitations, a low computational cost equivalent plate model can be used to evaluate the structural parameters for a wide range of wing configurations.

Appendix A Equivalent Plate Evaluation

The method used to reduce a two-dimensional structure into a simplified equivalent plate is presented here alongside a sample evaluation of a symmetric, NACA0010 [39] cross-section with a chord length of 1m and featuring a front and a rear spar. The wing skin for this evaluation is a composite skin with two layers of structural fabric with a thickness of 0.3mm each and with a 3mm piece of core in-between the two layers, the wing skin for the upper and lower surfaces are symmetric. The spar caps are made of a single layer of unidirectional fabric, that is 0.35mm thick while the spar webs have a thickness of 3mm. For each layer the area moment of inertia is determined by breaking the wing section into many straight lines, evaluating the effects of each point mass, and combining the total of each section. The effects of each point are defined using Eq.21, similarly to the method used to evaluate the boom area effects.

Once the initial area moments of inertia ($I_{xx,i}$ & $I_{yy,i}$) and the polar moment of inertia (J) is determined, the new layer positions and thicknesses can be calculated. The initial moments of inertia must be equal to the final moments of inertia for the equivalent plate idealization to be valid and therefore the moment of inertia for the new equivalent plate across the y-axis must be,

$$I_{xx,i} = I_{xx,new} = \frac{w_{new}^3 t_{new}}{12} + Ax^2, \quad x = 0$$

where the distance between the centerline and the center of the rectangle is (x). In this scenario the distance between the two is zero as the rectangle, along the x-axis, is centered on the y-axis. The initial moment of inertia, and the width of the rectangle (w_{new}) are known, allowing for the thickness (t_{new}) of the specific layer to be determined. Following this the displacement from the x-axis (y) is solved by using,

$$I_{yy,i} = I_{yy,new} = \frac{w_{new} t_{new}^3}{12} + A y^2$$

$$y = \sqrt{\frac{I_{yy,i} - \frac{w_{new} t_{new}^3}{12}}{A}}$$

For this example an wingbox width of 0.500m is selected, which represents the distance between the rear and the main spar as well as the equivalent plate width (w_{new}). The thickness and the distance of each layer from the centerline is:

$$\text{Top Layer} = 18.54\text{mm}$$

$$\text{Fabric, Layer 1} = 18.29\text{mm}$$

$$\text{Core, Layer 2} = 16.02\text{mm}$$

$$\text{Fabric, Layer 3} = 15.77\text{mm}$$

— — — Centerline — — —

where the layer location is the distance from the centerline to the closest portion of the equivalent layer thickness. The location of each equivalent later is found by equating the moment of inertia for the initial airfoil structure and an equivalent plate structure. The moment of inertia for each layer of the initial structure is found through,

$$I_{xx,layer 1} = \sum_{i=1}^n A y^2 = d_{ij} \cdot t_{layer 1} * y_{ij} \quad (24)$$

$$I_{xx,layer 1} = 3.54 \cdot 10^4 \text{mm}^4$$

where, n is the number of points along the surface of the airfoil and j is equal to the current point (i) plus 1. The thickness of the structural fabric layer, t , is related to the area of the section through the distance, d_{ij} , between points i and j . The mid-point between points i and j has a distance from the x-axis of y_{ij} . The moment of inertia across the y-axis is solved similarly to the x-axis.

$$I_{yy,layer 1} = \sum_{i=1}^n A x^2 = d_{ij} \cdot t_{layer 1} * x_{ij} \quad (25)$$

$$I_{yy,layer 1} = 2.66 \cdot 10^6 \text{mm}^4$$

The moment of inertia across both the x and the y axis are maintained between the initial airfoil cross-section and the equivalent plate. To determine the equivalent layer thickness and to determine the distance of the new equivalent layer from the x-axis.

$$\begin{aligned} t_{eq,layer\ 1} &= 0.248 \\ y_{eq,layer\ 1} &= 18.29 \end{aligned} \tag{26}$$

Appendix B Idealized Shear Center Location

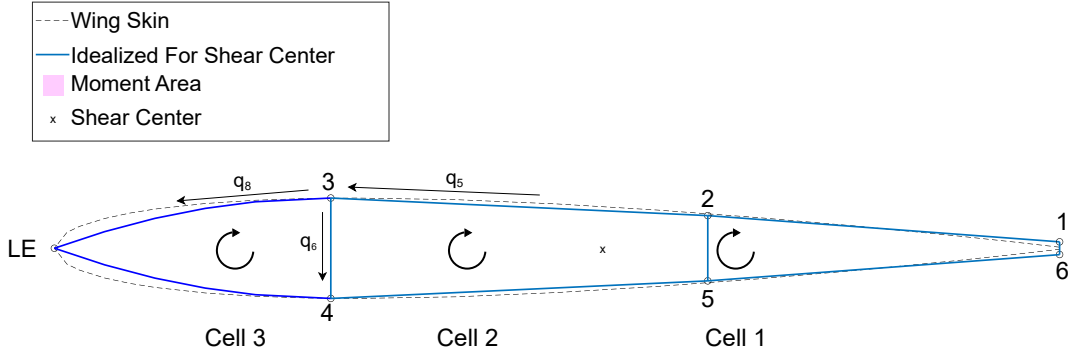


Figure B.1 NACA0010 Structural idealization.

To evaluate the shear center for a two-dimensional wing section the wing skin and the spars are estimated through the placement of booms at the points of intersection. These points, shown in Fig.1, represent the proportional area affects of the adjacent wing sections that reflect the relative shear effects of the different materials in the varying sections. The evaluation uses the following shear moduli for the wing skin and spars:

$$G_{Wing\ Skin} = 11.3 kPa$$

$$G_{Spar\ Web} = 11.0 kPa$$

$$G_{Spar\ Cap} = 2.0 kPa$$

The calculation of the shear center, through structural idealization, is dependent on the geometry of the wing section and on the shear modulus of the different sections. The idealized boom areas for boom j is,

$$B_j = \sum \left[t \frac{W}{6} \left(2 + \frac{y_i}{y_j} \right) \right]_{spar} + \sum \left[t \frac{W}{6} \left(2 + \frac{y_k}{y_j} \right) \right]_{skin} \quad (27)$$

where, i and k represent adjacent points across a spar or skin component with a known length (W) and component thickness (t). The boom areas are then used to calculate the polar moment of inertia effects of each point based on the distance of the boom node

from the x-axis. In this scenario the shear center is assumed to be near the centerline of the selected thin airfoil however, this assumption limits this estimation to low chamber airfoils. The moment arm of each boom is used in a later stage to evaluate the shear flow.

At each boom location the shear flow is evaluated by equating the shear flow in to the shear flow out, allowing for a system of equations to be developed based on the shear flow through each cell in the structure. In the case of the presented NACA0010 airfoil there are three cells, the leading edge, trailing edge, and in between the two spars. Each cell is considered to have a clockwise rotational frame. The system of equation to solve for the shear flow through the wall lengths for each cell is:

$$\begin{aligned} \frac{B_2 y_2 W_{25}}{G_{spar}} + \frac{B_6 y_6 W_{61}}{G_{skin}} &= -q_1 \left(\frac{W_{12} + W_{56} + W_{61}}{G_{skin}} + \frac{W_{25}}{G_{spar}} \right) + q_5 \left(\frac{W_{25}}{G_{spar}} \right) \\ 0 &= -q_5 \left(\frac{W_{25}}{G_{spar}} \right) + q_8 \left(\frac{W_{34}}{G_{skin}} + \frac{W_{34}}{G_{spar}} \right) \\ \frac{B_3 y_3}{G_{spar}} &= q_1 \left(\frac{W_{25}}{G_{spar}} \right) - q_5 \left(\frac{W_{23} + W_{45}}{G_{skin}} + \frac{W_{34} + W_{25}}{G_{spar}} \right) + q_8 \left(\frac{W_{34}}{G_{spar}} \right) \end{aligned} \quad (28)$$

The shear flow through each resulting section is determined and can be used to find the shear center. The shear center represents a location where the bending and twisting effects on a wing section are decoupled, meaning that the twist effects must be zero under pure bending. Based on this, a point e , is selected to represent the shear center as a distance from the trailing edge. The shear center can be found by taking the moment effects of the shear flow through across the moment arm, represented as a triangular area as shown in Fig.2. The shear center, as a result of the geometry and the shear modulus of each section is found through,

$$e = \frac{\sum_{i=2}^N (2A_i \cdot q_i)}{I} \quad (29)$$

where, A_i is the triangular area between $i = 1$ and the wall length being evaluated as shown in Fig.2. The summation of the moment arm due to the shear flow across a number of elements, N , allows for the location where the moment is zero to be found. The represented structural idealization is used for materials that do not have internal material coupling, such as isotropic materials or composite fabrics oriented at [-45/45] or [0/90].

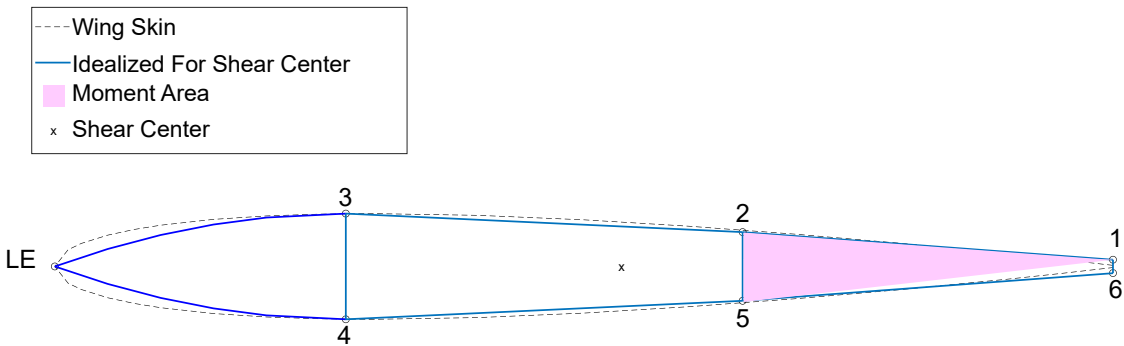


Figure B.2 Triangular moment arm for shear center evaluation for nodes 2 to 5.

Appendix C Aeroelastic Model Input Example

The following section discusses and defines the various input parameters required to run the aeroelastic model and the aeroelastic optimization both described in Chapter 3. The input parameters defined are defined in S.I. units (meters, kg, etc.). The following example input file defines the geometry, structural parameters, aerodynamic conditions (including gust conditions) and the frames of reference required to evaluate the selected aircraft:

File Type: .VAP

<VAP>

```
<settings>
    <relax>(TRUE/FALSE, toggle relaxed wake evaluation)</relax>
    <steady>(TRUE/FALSE, toggle steady state evaluation)</steady>
    <maxtime>{seconds , define max simulation time}</maxtime>
    <delta_time>{seconds , define aerodynamic timestep}</delta_time>
    <start_forces>(timestep , start aerodynamic forces)</start_forces>
    <stiff_wing>(1/0, toggle rigid wing evaluation)</stiff_wing>
    <fixed_lift>(1/0, toggle fixed lift evaluation)</fixed_lift>
    <gust_mode>(set gust: sine(1) , 1-cosine(2) , Sharp-Edge(3)
    <gliding>(TRUE/FALSE, toggle gliding evaluation)</gliding>
    <viscous>(TRUE/FALSE, toggle viscous corrections)</viscous>
    <flightdynamics>(TRUE/FALSE, toggle model)</flightdynamics>
</settings>

<conditions>
    <density>(kg/m^3 , define constant fluid density)</density>
    <kin_viscosity>(m^2/s , kinematic viscosity )
```

```
<gust_amplitude>(m/s , max gust amplitude)</gust_amplitude>
<gust_length>(m, length of gust encountered)</gust_length>
<gust_start>(timestep , begin gust effects)</gust_start>
</conditions>
```

```
<vehicle>
```

```
<global_x>(m, location of wing)</global_x>
<global_y>(m, location of wing)</global_y>
<global_z>(m, location of wing)</global_z>
```

```
<vehicle_CG>
```

```
<x>(m, location of wing CG from global)</x>
<y>(m, location of wing CG from global)</y>
<z>(m, location of wing CG from global)</z>
</vehicle_CG>
```

```
<speed>(m/s , set cruise speed)</speed>
<weight>(kg , complete aircraft mass)</weight>
<interference_drag>(N, addition drag)</interference_drag>
<alpha>(degree , starting AoA)</alpha>
<fpa>(degree , starting flight path angle)</fpa>
<roll>(degree , starting roll angle)</roll>
<ref_area>(m^2 , reference planform area)</ref_area>
<ref_span>(m, reference wingspan)</ref_span>
<ref_cmac>(m, reference mean chordlength)</ref_cmac>
```

```
<wing>
```

```

<symmetry>(TRUE/FALSE, toggle left/right wing symmetry)</symmetry>
<incidence>(degree, incidence angle of wing)</incidence>
<trimable>(TRUE/FALSE, toggle on for trimming wing)</trimable>
<flexible>(TRUE/FALSE, toggle rigid wing)</flexible>
<triangular_elements>(TRUE/FALSE, triangular structural elements)
<mass>(kg, portion of total mass from the wings)</mass>
<chordwise_elements>(#, set chordwise elements)

```

<CG>

```

<x>(m, distance from global)</x>
<y>(m, distance from global)</y>
<z>(m, distance from global)</z>

```

</CG>

<panel>

```

<spanwise_elements>(#, set spanwise elements)</spanwise_elements>
<strip_airfoil>(file, select airfoil data file)</strip_airfoil>

```

<section>

```

<wing_x>(m, section start location from centerline)</wing_x>
<wing_y>(m, section start location from centerline)</wing_y>
<wing_z>(m, section start location from centerline)</wing_z>
<chord>(m, chordlength for section start)</chord>
<twist>(degree, twist angle at section start)</twist>

```

</section>

</panel>

</wing>

```

<structure>
  <conditions>
    <valSDELTIME>0.0005</valSDELTIME>
    <valNSELE>(#, spanwise structural elements +1)</valNSELE>
    <valSTIFFSTEPS>(#, define number of rigid timesteps)
  </conditions>

  <properties>
    <stiffness>
      <A_vecEIx>(Pa*m^2, exponential change in EI spanwise)</A_vecEIx>
      <B_vecEIx>(Pa*m^3, linear change in EI spanwise)</B_vecEIx>
      <C_vecEIx>(Pa*m^4, constant EI)</C_vecEIx>
    </stiffness>

    <geometry>
      <A_vecEA>(% chord/m^2, exponential change in SC)</A_vecEA>
      <B_vecEA>(% chord/m, linear change in shear center)</B_vecEA>
      <C_vecEA>(% chord, constant shear center)</C_vecEA>
    </geometry>

    <mass>
      <C_vecJt>(m^4, polar moment of inertia)</C_vecJt>
      <C_vecLM>(kg/m, linear mass distribution)</C_vecLM>
    </mass>
  </properties>
</structure>

```

```

<fuselage>
    <mass>(kg, portion of total mass from fuselage)</mass>
    <length>(m, length of rectangular fuselage)</length>
    <valNFELE>(#, number of elements)</valNFELE>
    <flat_plate_area>(m^2, surface area of fuselage)</flat_plate_area>
</fuselage>

</vehicle>
</VAP>
```

Note that the aerodynamic timestep must be based on the following:

$$<delta_time> = \Delta t = \frac{c}{(c_{elements}) \cdot (V_\infty)}$$

Appendix D Optimized Aircraft Configuration

Table D.1 Optimized and segmented SW117 aircraft configurations.

Spanwise Location (m)		Optimized Configuration	Segmented Configuration
0.17	EI ($kN \cdot m^2$)	8.8	9.0
	GJ ($kN \cdot m^2$)	6.2	6.1
	SC (%c)	0.54	0.53
0.34	EI ($kN \cdot m^2$)	8.8	9.0
	GJ ($kN \cdot m^2$)	6.2	6.1
	SC (%c)	0.54	0.53
0.51	EI ($kN \cdot m^2$)	8.8e	9.0
	GJ ($kN \cdot m^2$)	6.2	6.1
	SC (%c)	0.54	0.53
0.68	EI ($kN \cdot m^2$)	9.5	9.0
	GJ ($kN \cdot m^2$)	5.8	6.1
	SC (%c)	0.53	0.53
0.85	EI ($kN \cdot m^2$)	8.9	9.0
	GJ ($kN \cdot m^2$)	5.7	6.1
	SC (%c)	0.53	0.53
1.02	EI ($kN \cdot m^2$)	9.5	9.0
	GJ ($kN \cdot m^2$)	6.1	6.1
	SC (%c)	0.51	0.53
1.19	EI ($kN \cdot m^2$)	9.7	8.5
	GJ ($kN \cdot m^2$)	6.4	6.7
	SC (%c)	0.50	0.48
1.36	EI ($kN \cdot m^2$)	9.0	8.5
	GJ ($kN \cdot m^2$)	6.4	6.7
	SC (%c)	0.49	0.48
1.53	EI ($kN \cdot m^2$)	8.6	8.5
	GJ ($kN \cdot m^2$)	6.9	6.7
	SC (%c)	0.47	0.48
1.70	EI ($kN \cdot m^2$)	8.7	8.5
	GJ ($kN \cdot m^2$)	6.9	6.7
	SC (%c)	0.48	0.48
1.87	EI ($kN \cdot m^2$)	9.4	8.5
	GJ ($kN \cdot m^2$)	6.5	6.7
	SC (%c)	0.48	0.48
2.04	EI ($kN \cdot m^2$)	9.6	9.6
	GJ ($kN \cdot m^2$)	6.8	6.8
	SC (%c)	0.48	0.48
2.19	EI ($kN \cdot m^2$)	9.6	9.6
	GJ ($kN \cdot m^2$)	6.7	6.8
	SC (%c)	0.50	0.48
2.36	EI ($kN \cdot m^2$)	9.6	9.6
	GJ ($kN \cdot m^2$)	6.8	6.8
	SC (%c)	0.48	0.48
2.53	EI ($kN \cdot m^2$)	9.6	9.6
	GJ ($kN \cdot m^2$)	6.8	6.8
	SC (%c)	0.48	0.48
2.70	EI ($kN \cdot m^2$)	9.7	9.6
	GJ ($kN \cdot m^2$)	6.8	6.8
	SC (%c)	0.48	0.48

Appendix E Effect of Manufacturing Irregularities

Composite manufacturing techniques, such as resin infusion, involve the hand placement of structural fabrics, resulting in limited fiber orientation accuracy and precision. Manufacturing defects and human error during the placement of composite plies may result in small irregularities in ply orientation. Small shifts in the ply orientation result in a change in the structural performance for the given aircraft configuration resulting in a change in gust energy harvesting potential.

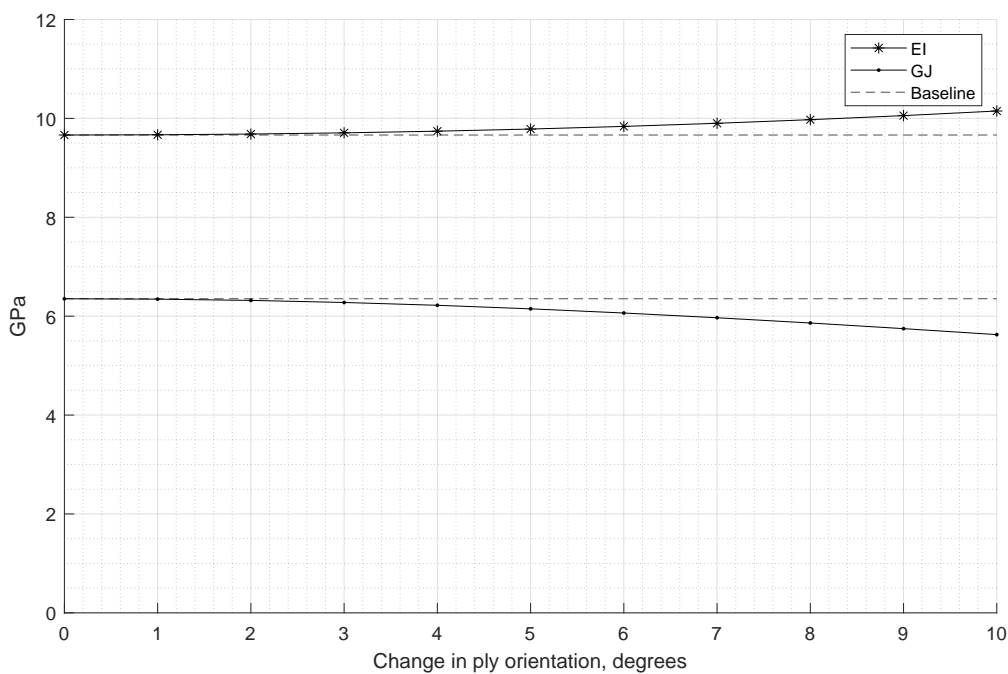


Figure E.1 Sensitivity of manufacturing irregularities on structural parameters.

Small changes in ply orientation can result in changes in the stiffness parameters of the wing. For a wing configuration with four plies of a structural weave oriented at [-45/45] that experiences a 5 degree misalignment, a change of 3.2% in torsional rigidity and 1.3% in bending stiffness was seen as shown in Fig. 1. Depending on the reliability of the placement methods used and the precision in the manufactured components, significant changes, greater than 5%, are seen if the plies are misaligned at angles larger than 5 degrees. When considering the accuracy of the components and the design of the structures, minor gains in performance may not reliably be achievable. For example, an irregularity of 10 degrees in the ply orientation resulted in a change in the gust energy altitude gains for the baseline aircraft configuration of 26% while within a 2 m/s sinusoidal gust.

References

- [1] M. Melville, “Aeroelastic wing design for gust energy harvesting,” Ph.D. dissertation, Toronto Metropolitan University, Toronto, Canada, 2023.
- [2] M. Melvile, “Modeling of gust energy extractions through aeroelastic tailoring,” *Master’s Thesis, Toronto Metropolitan University*, 2018.
- [3] M. Melville, G. Bramesfeld, A. Kolaei, and H. Alighanbari, “Aeroelastic tailoring gust-energy extraction,” *Journal of Aerospace Engineering, Vol 23*, 2020.
- [4] D. Ironside and G. Bramesfeld, “Modeling of wing drag reductions due to structural dynamics in atmospheric gusts,” *AIAA 28th Applied Aerodynamics Conference*, no. 4683, 2010.
- [5] N. Gavrilovic, B. Kirsch, G. Abrantes, P. Pastor, and E. Benard, “Passive gust energy extraction of small uavs,” *53nd 3AF International Conference on Applied Aerodynamics*, 2018.
- [6] D. Heathcote, “Aerodynamic load alleviation using mini-tabs,” Ph.D. dissertation, University of Bath, 2017.
- [7] G. Huang, Y. Dai, C. Tang, C. Huang, and X. Zuo, “Gust energy harvesting of a free-flying aircraft model by cfd/csd simulation and wind tunnel testing,” *Journal Aerospace Engineering*, vol. 35, 2022.
- [8] J. Dillsaver, Matthew, “Gust response and control of very flexible aircraft,” Ph.D. dissertation, University of Michigan, 2013.
- [9] G. Sachs, J. Traugott, and A. P. Nesterova, “Flying at no mechanical energy cost: disclosing the secret of wandering albatrosses,” *PLoS ONE*, 2012.
- [10] D. J. Sherman, “Extreme vertical gusts in the atmospheric boundary layer,” Australian Government Defense Science and Technology Group, Tech. Rep., 2015.

- [11] D. o. T. Federal Aviation Administration, *Gust and Turbulence Loads*, 25.341, Code of Federal Regulations, Washington, USA, 2024.
- [12] J. Etele, “Overview of wind gust modelling with application to autonomous low-level uav control,” Defense RD Canada, Tech. Rep., 2006.
- [13] A. Nath, R. Anand, J. Desai, M. Sultan, and S. Aravind Raj, “Modelling and finite element analysis of an aircraft wing using composite laminates,” *International Conference on Advanced Materials and Modern Manufacturing*, no. 1183, 2024.
- [14] M. T. Bordogna, P. Lancelot, D. Bettebghor, and R. D. Breuker, “Static and dynamic aeroelastic tailoring with composite blending and manoeuvre load alleviation,” *Structural and Multidisciplinary Optimization*, 61:2193–2216, vol. 61, 2020.
- [15] R. L. Bisplinghoff, H. Ashley, and R. L. Halfman, *Aeroelasticity*. Dover Publications, 1996.
- [16] D. P. Raymer, *Aircraft Design: A Conceptual Approach*, Seventh Edition. American Institute of Aeronautics and Astronautics, Inc, 2024.
- [17] J. Allen, *Glider Handbook*. Federal Aviation Administration, 2013, ch. 9.
- [18] J. R. Wright and J. E. Cooper, *Introduction to Aircraft Aeroelasticity and Loads*. Wiley, 2008.
- [19] Y. Liu, “Comparison of the passive and active control gust alleviation of a flying-wing aircraft,” *19th International Conference of Fluid Power and Mechatronic Control Engineering*, 2018.
- [20] Y. Cheng, D. Li, and J. Xiang, “Efficiency evaluation of energy harvesting from discrete gust response for plate wing,” *Journal of Sound and Vibration*, 2020.
- [21] R. Abbott, *Analysis and Design of Composite and Metallic Flight Vehicle Structures*. Abbot Aerospace UK LTD, 2019.

- [22] C. Monroy, A. Skordos, and M. Sutcliffe, “Design selection methodology for composite structures,” *Materials Design Journal (1980-2015)*, 2008.
- [23] S. A. Brent, *Fundamentals of Composite Manufacturing, Second Edition*. Society of Manufacturing Engineers, 2008, ch. 12-13.
- [24] M. Pogosyan, E. Nazarov, V. Koroliskii, N. Turbin, and K. Shramko, “Aircraft composite structures integrated approach: a review,” *Journal of Physics: Conference Series*, 2020.
- [25] S. Kilimtzidis, A. Kotzakolios, and V. Kostopoulos, “An efficient optimization scheme for the preliminary sizing of composite aircraft wings,” *International Forum on Aeroelasticity and Structural Dynamics*, 2022.
- [26] G. Giles, “Equivalent plate analysis of aircraft wing box structures with general planform geometry,” NASA Technical Memorandum, Tech. Rep., 1986.
- [27] J. N. Reddy, *Introduction to the Finite Element Method, 4th Edition*. McGraw-Hill Education, 2019.
- [28] G. Bramesfeld and M. D. Maughmer, “Relaxed-wake vortex-lattice method using distributed vorticity elements,” *Journal of Aircraft, 45th Edition*, vol. 45, 2008.
- [29] J. Cole, M. D. Maughmer, M. Kinzel, and G. Bramesfeld, “Unsteady lift prediction with a higher-order potential flow method,” *MDPI: Aerospace*, vol. 7, 2020.
- [30] J. K. Seo, B. J. Kim, H. S. Ryu, Y. C. Ha, and J. K. Paik, “Validation of the equivalent plate thickness approach for ultimate strength analysis of stiffened panels with non-uniform plate thickness,” *Thin-Walled Structures, Volume 49*, 2011.
- [31] *MatWeb: Material Property Data*, Automation Creation Inc., <https://www.matweb.com>, accessed: 09-06-2024.

- [32] B. Y. Zeyrek, F. Oztruk, B. Aydogan, and E. Dilekcan, “Review of thermoplastic composites in aerospace industry,” *International Journal on Engineering Technologies and Informatics*, 2022.
- [33] R. Sullivan, M. Rohani-Rais, T. Lacy, and N. Alday, “Structural testing of an ultra-light uav composite wing,” *47th AIAA Structures, Structural Dynamics, and Materials Conference*, 2006.
- [34] “Superwake,” <https://www.superwake.ca/>, accessed: 2024-09-30.
- [35] S. N. Sivanandam, *Introduction to Genetic Algorithms*. Springer Berlin/Heidelberg, 2007.
- [36] B. J. Bacon and I. M. Gregory, “General equations of motion for a damaged asymmetric aircraft,” *AIAA Atmospheric Flight Mechanics Conference and Exhibit*, 2007.
- [37] F. Hartshorn, “Analysis of asymmetric aircraft aerodynamics due to an experimental wing glove,” *29th AIAA Applied Aerodynamics Conference*, 2011.
- [38] B. L. Larrimer, *Thinking Obliquely*. NASA Aeronautics Book Series, 2013.
- [39] I. H. Abbott, A. E. Doenhoff, and L. S. Stivers Jr, “Summary of airfoil data,” National Advisory Committee for Aeronautics, Tech. Rep., 1945.